Rheologica Acta (2024) 63:493–512
https://doi.org/10.1007/s00397-024-01454-y

ORIGINAL CONTRIBUTION

Magnetic field-dependent rheological behavior of thermoresponsive poly(N-isopropylacrylamide) solutions

Christopher A. P. Neal[1] · Abhishek M. Shetty[2] · Jason D. Linn[1] · Michelle C. Quan[1] · Joseph D. Casas[3] · Michelle A. Calabrese[1]

Received: 11 March 2024 / Revised: 22 April 2024 / Accepted: 1 May 2024 / Published online: 30 May 2024

Abstract

Magnetic (**B**) fields are an intriguing route for manipulating soft materials. While most research on **B** field manipulation of diamagnetic polymers has focused on alignment of ordered structures or anisotropic domains, our recent work uncovered a previously unrecognized effect: **B** fields alter hydration and hydrogen bonding in thermoresponsive poly(N-isopropylacrylamide) (PNIPAM) solutions. Despite the well-known thermoreversible coil-to-globule transition and hydrogel formation upon heating, the impact of magnetic fields on these structural and rheological transitions has been largely unexplored. In this study, we thoroughly examined the temperature-dependent magnetorheology of PNIPAM solutions, varying **B** field strength, polymer content, and molecular weight. Linear magnetorheology reveals that increasing the **B** field intensity decreases the dynamic moduli of the resulting physical hydrogel, across polymer concentrations (5–20% wt) and molecular weights (30–108 kDa), by up to an order of magnitude. Conversely, the gelation onset temperature does not change substantially. This weakening effect is more pronounced at longer magnetization times and slower temperature ramp rates. Nonlinear magnetorheology following hydrogel formation reveals a two-step yielding process characteristic of attractive-driven glasses, suggesting that magnetization decreases both the stress and length scales associated with mesoglobule cage breaking. We propose that **B** fields impact the hydrogel rheology by altering the mesoglobule size and water content. This work uncovers essential understanding of how **B** fields alter hydrogel formation in PNIPAM solutions, broadening the scope of magnetic field manipulation of diamagnetic polymer solutions.

Keywords Magnetorheology · Hydrogel · PNIPAM · Solvation · Yielding

Introduction

Stimuli-responsive materials that adapt their conformations and macroscopic properties in response to external stimuli are foundational to the future of advanced electronics such as flexible displays (Peumans and Forrest 2001; Kim et al. 2010; Cao and Rogers 2009), biosensors (Tokarev and Minko 2009), thin-film photo-responsive solar cells (Shaheen et al. 2001; Granström et al. 1998; Peumans et al. 2003), and organic light emitting diodes (Forrest 2004) among other applications. These materials possess the remarkable ability to actively respond to changes in external stimuli such as temperature, pH (Dai et al. 2008), magnetic fields (Thévenot et al. 2013; Osuji et al. 2004; Hamley et al. 2004; de Gennes and Pincus 1970; Wang et al. 2015; Takahashi et al. 2006) and electric fields (Kuijk et al. 2011; Shah et al. 2014) to alter their micro- or nano-structure in real-time (Wei et al. 2017; Bril et al. 2022). These responses in turn lead to a change in physical properties such as mechanical strength (Buwalda et al. 2014; Kimura et al. 2002; Andrews et al. 1999), optical clarity (He et al. 2010; Asher et al. 1994; Pan et al. 1998), color (Maji et al. 2016), or other properties which can be utilized in a wide variety of applications.

One of the most widely studied thermoresponsive soft materials is aqueous poly(N-isopropylacrylamide) (PNIPAM), which exhibits a lower critical solution temperature (LCST) around biologically relevant temperatures. Above a

✉ Michelle A. Calabrese
mcalab@umn.edu

1 Department of Chemical Engineering and Materials Science, University of Minnesota, Twin Cities, Minneapolis 55455, MN, USA

2 Rheology Division, Anton Paar, Ashland 23005, VA, USA

3 Department of Mechanical Engineering, University of Texas, Rio Grande Valley, Edinburg 78539, TX, USA

temperature of ~32 °C, PNIPAM undergoes a coil-to-globule conformational transition accompanied by demixing of the polymer from water. Here, a fraction of hydrogen bonds between PNIPAM and water are liberated and new PNIPAM-PNIPAM and water-water hydrogen bonds form, partially dehydrating the polymer chains. Following this partial dehydration, hydrophobic interactions between PNIPAM chains lead to chain aggregation and the formation of PNIPAM-rich, colloidally stable mesoglobules of size ~100 nm (Lang et al. 2018; Balu et al. 2007; Niebuur et al. 2019a). Small-angle neutron scattering (SANS) and dissipative particle dynamics (DPD) simulations have also confirmed the presence of solvated PNIPAM aggregates below the phase transition temperature that may aid in the formation of these PNIPAM mesoglobules (Lang et al. 2018). Direct imaging and SANS reveal that these mesoglobules resemble colloidal particles, as the globules are spherical in shape and form sharp interfaces (Balu et al. 2007; Niebuur et al. 2019a). The size of the PNIPAM mesoglobule particles at elevated temperatures depends on concentration, molecular weight, temperature, and heating rate (Wu et al. 2004; Gorelov et al. 1997; Niebuur et al. 2019a). However, these mesoglobules are typically large enough to prevent light transmittance; as a result, this structural and optical transition is often examined via turbidimetry (Aseyev et al. 2005; Halperin et al. 2015).

Above a critical PNIPAM concentration, the PNIPAM mesoglobules form a physical hydrogel network, which is structurally and rheologically similar to suspensions of PNIPAM microgel particles beyond their dehydration temperature (Ikeda et al. 2013; Pellet and Cloitre 2016; Scotti et al. 2020). According to mode-coupling theory (MCT), short-ranged attractive interactions between repulsive particles (i.e., PNIPAM mesoglobules or microgel particles) entrap the particles in cages constrained by nearest-neighbor "bonds," known as an attractive-driven glass (ADG) or "gel" at lower volume fractions (Pusey 2008; Zaccarelli and Poon 2009; Pham et al. 2004). Thus, mesoglobules in an attractive glass will be constrained both by direct interactions with nearby mesoglobules and by caging constraints, producing a relatively weak but stable hydrogel network (Pusey 2008; Franco et al. 2021).

Tuning the PNIPAM hydrogel properties by altering either the interactions between mesoglobules or the longer-range connectivity in the ADG can expand the potential applications for PNIPAM materials. Due to its LCST around biologically relevant temperatures, PNIPAM has previously been studied as a tool for gene and drug delivery, cell cultures (Shimizu et al. 2001), thermally responsive polymer-protein conjugates (Bulmus et al. 2000; Lee and Park 1998; Hoffman et al. 2000), and other biologically related smart hydrogel applications (Xia et al. 2013). In many cases, the dramatic change in PNIPAM solution elasticity with small temperature changes is critical. However, control over the properties of these hydrogels usually requires changes in the solution composition, such as changes in solution pH (Garbern et al. 2010) or through copolymer (Uchida et al. 2019; Smith et al. 2021) or nanoparticle incorporation (Tan et al. 2010; Neal et al. 2023b). These additives increase the system complexity and in biomedical applications, can lead to time-consuming and costly regulatory reviews. Instead, non-destructive external stimuli such as magnetic (**B**) fields can provide a homogeneous, contactless stimulus to tune material properties without altering chemical composition.

In soft and polymer materials, **B** fields have typically been used to reorient or order ferromagnetic or superparamagnetic nanoparticles suspended in polymer matrices, for example in magnetorheological elastomers (MRE) (Jolly et al. 1996; Filipcsei et al. 2007). Here, **B** fields can induce dipole-dipole interactions in magnetically responsive nanoparticles, causing nanoparticle chain formation in the **B** field direction. Diamagnetic materials can also respond to **B** fields, driven by alignment of anisotropic constituents such as liquid crystalline side groups (Osuji et al. 2004; Gopinadhan et al. 2012) or crystallization of hydrocarbon chains (Vshivkov et al. 2017, 2020). For example, in diamagnetic polyelectrolyte solutions, **B** fields can increase the crystallization and phase separation temperature due to altered orientation and interactions between constituents (Vshivkov et al. 2017, 2020).

Previous work of ours and others has demonstrated that **B** fields critically impact the behavior of solvents and polymer solutions. Vshivkov and coworkers examined **B** field-induced changes in polyelectrolyte crystallization, finding that **B** field effects were diminished in higher polarity solvents (Vshivkov et al. 2017, 2020). In pure water, **B** fields have been shown to alter hydrogen bonding and the structure of hydrogen-bonded water clusters, leading to changes in macroscopic properties such as specific heat capacity, boiling point, and viscosity (Pang and Deng 2008a; Esmaeilnezhad et al. 2017; Pang and Deng 2008b; Wang et al. 2018; Selim and El-Nady 2011; Pang 2006; Zhou et al. 2017; Bakherad et al. 2017; Ghorbani et al. 2019). **B** field application induces changes in the electron polarization of water molecules, leading to significant changes in molecular vibrations and the hydrogen bond strength (Pang and Deng 2008b, a; Pang 2006). Similarly, Sronsri et al. observed changes in the Raman and infrared spectra of water due to magnetization, which depended on the duration of magnetization and intensity of the applied **B** field (Sronsri et al. 2021. Pang and Bo also found that **B** fields increase the dielectric constant of water (Pang and Deng 2008b), potentially increasing the Debye screening length of colloids in suspension. Accordingly, magnetizing aqueous PNIPAM solutions may alter the mechanism of dehydration, aggregation and hydrogel network formation upon temperature elevation.

Previously, we reported that **B** fields decrease the optical clouding temperature and thermodynamic phase transition

enthalpy in PNIPAM solutions due to complex changes in the solution H-bonding environment (Neal et al. 2023a). Here, **B** fields had less impact on the transition enthalpies at higher polymer contents and no enthalpy changes were observed above 6% polymer, which was attributed to reduced polymer hydration at higher polymer contents. Interestingly, limited rheological tests on 10% polymer solutions suggested that despite the absence of measurable enthalpy differences, **B** fields could alter physical hydrogel formation in 10% PNIPAM solutions (Neal et al. 2023a). However the mechanism by which **B** fields alter physical hydrogel formation — and the robustness of this unique **B**-altered behavior to parameters like field intensity, molecular weight, and polymer content — was not established.

To gain a more thorough understanding of how magnetic fields impact physical hydrogel formation in PNIPAM, here we use magnetorheology to explore a range of aqueous PNIPAM solutions in the semi-dilute through concentrated regimes. Specifically, we examine the effects of **B** field strength, polymer molecular weight and concentration, and rheological parameters such as geometry and temperature ramp rate to understand how **B** fields alter the gelation of PNIPAM solutions upon temperature elevation. Despite these wide-ranging sample and experimental parameters, we obtain qualitatively similar results across systems which demonstrate that **B** fields consistently decrease the dynamic moduli of PNIPAM hydrogels — with magnetic effects maximized using slow temperature ramp rates. Finally, the nonlinear rheological behavior of magnetized hydrogels reveals how **B** fields alter mesoglobule interactions and subsequent hydrogel yielding behavior. Beyond providing a new route for tailoring the properties of PNIPAM solutions, these studies provide new fundamental insight on how molecular-level field-induced changes to solvation in polymer solutions subsequently manifest on longer length scales to create unique rheological behaviors.

Methodology

Polymerization and characterization

Poly(*N*-isopropylacrylamide) was polymerized via reversible addition-fragmentation chain transfer, using 2-(ethylsulfanyl thio-carbonylsulfanyl)-2-methyl propionic acid (EMP) as the chain transfer agent. EMP was synthesized following prior protocols (Linn et al. 2022). *N*-isopropylacrylamide (NIPAM, Fisher Scientific, 98%, stabilized) was purified via sublimation and dried under vacuum. Azobisisobutyronitrile (AIBN, Sigma-Aldrich, 98%) was recrystallized from methanol three times and dried under vacuum.

PNIPAM homopolymers are referred to as P59 ($M_n \approx 59$ kDa, $Đ \approx 1.23$), P108 ($M_n \approx 108$ kDa, $Đ \approx 1.13$), and P30 ($M_n \approx 30$ kDa, $Đ \approx 1.06$) (see Sec. SI.1.1 and Sec. SI.1.2 for characterization). Vibrating sample magnetometry (Sec. SI.1.3) confirmed diamagnetism of all materials. All concentrations reported are on a percent weight of total weight basis (% (w/w)). Dry polymer was added to a vial followed by the appropriate mass of HPLC-grade water. Solutions were vortexed and mixed in a refrigerator for 48 h before use.

Differential scanning calorimetry

Thermodynamic phase transition temperatures and enthalpies were quantified using a TA Instruments DSC Q2000 and hermetically sealed aluminum Tzero pans loaded with ~ 20 mg of PNIPAM solution. Pans were loaded onto the instrument at 10 °C and equilibrated for 1 min. Heat flow was quantified as a function of temperature upon heating from 10 °C to 50 °C at a rate of 1 °C/min (0.2 °C/min also used, where noted). Heat flow data was baseline-corrected using a tangential sigmoid model described previously (Neal et al. 2023a) and available through the TA Instruments Universal Analysis software. Phase transition enthalpy was calculated as the integral of heat flow as a function of time upon heating (see Sec. SI.2, Fig. S6a). Thermodynamic phase transition onset ($T_{on,DSC}$) and peak ($T_{peak,DSC}$) temperatures were extracted as the onset of the thermal transition and the peak in heat flow as calculated by this software. Replicates of DSC experiments are provided in Sec. SI.3.

Turbidimetry

Optical transition temperatures of PNIPAM solutions were quantified using an in-house turbidimeter described previously (Neal et al. 2023a). In short, transmittance was examined using a red laser (5 mW, class 3R, 650 nm) and a standard CdS photoresistor while using a cartridge heater and PTD thermocouple controlled by an Arduino Uno to control temperature. Solutions were heated from 20 °C to 40 °C at respective temperature ramp rates. Optical transition onset temperatures, T_{CP}, were quantified as the temperature at which the transmittance rate changed most with respect to temperature (Sec. SI.2, Fig. S6b). Turbidimetry replicates are in Sec. S1.4.

Dynamic light scattering

Hydrodynamic radii, R_h, of individual polymer chains at 25 °C were quantified using a Malvern Zetasizer dynamic light scattering (DLS) instrument. Dilute (0.1% (w/w)) PNIPAM solutions were filtered through 0.2 μm wwPTFE filters into

poly(methyl methacrylate) (PMMA) semi-micro (~800 μL) cuvettes. Scattering was collected over 50 scans of 10 s/scan at 25 °C. See Sec. SI.5 for autocorrelation curves and size distributions. Intrinsic viscosity and concentration regimes are estimated at 25 °C in Sec. SI.6 and Sec. SI.7.

Oscillatory rheological temperature ramps

Commercially available measuring systems for magnetorheological devices (MRDs) typically utilize parallel plate (PP) geometries due to their use with magnetorheological elastomers and meso-scale particulates. These PP geometries are not ideal for solution and hydrogel rheology. As such, an MRD-compatible cone-and-plate geometry was developed by Anton Paar to address these issues and reduce sample volume. This geometry has a 19.95 mm diameter cone (CP20), with a 1.996° cone angle and 86 μm truncation gap, enabling a 70 μL calculated sample volume vs. 160 μL in a 20 mm parallel-plate (PP20, 0.5 mm gap).

Physical hydrogel formation was quantified via small-amplitude oscillatory shear temperature ramps; both the CP20 and PP20 geometries were employed. Chilled solutions were deposited (100 μL for CP20; 200 μL for 0.5 mm gap PP20) onto an Anton Paar MCR 702 rheometer with a MRD180/1T accessory at 20 °C. Temperature was controlled via an external recirculator (Julabo FH32) filled with 40% vol. ethylene glycol aqueous solution; to counteract inductive heating from the electromagnet, extensive calibrations have been conducted to ensure consistent and comparable temperature settings.

First, solutions were sheared at 10 s^{-1} for 3 min to ensure sample homogeneity. Subsequently, solutions were allowed to relax for 3 min at 0.1%, 0.1 rad·s^{-1}. Next, **B** fields between 0 and 0.6 T were applied and G' and G'' were recorded at γ_0 = 0.1% and ω = 1 rad·s^{-1} from 20 °C to 40 °C (0.2 °C/min). The onset of the rheological transition, $T_{on,rheo}$, was defined as the intersection of a tangent through the point of maximum slope in modulus ($\partial G/\partial T\,|_{\max}$) and the low-temperature (20–28 °C) moduli. Where applicable, the maximum storage and loss moduli ($G'_{\max}$ and $G''_{\max}$, respectively) were defined as the maximum moduli achieved during temperature ramps, occurring at temperatures $T_{G'_{\max}}$ and $T_{G''_{\max}}$, respectively (Fig. S6c). Where shown, error bars on temperature ramps are the standard deviation of multiple trials ($n \geq 2$); see Sec. SI.9 for replicates.

Where necessary, caps filled with water were placed underneath the magnetic yoke to humidify the airspace and limit evaporation (Sec. SI.10). Most trials (≤10% PNIPAM) showed no difference with and without evaporation control (EC); see control trials with 10% P59 (Sec. SI.10). However, EC was employed for higher concentration solutions as a precaution.

Physical hydrogel amplitude sweeps

Following oscillatory temperature ramps ("Oscillatory rheological temperature ramps"), solutions were allowed to rest for 10 min under a low-amplitude (γ_0 = 0.1%, ω = 1 rad·s^{-1}) oscillations to allow for thermal and structural equilibration. Subsequently, amplitude sweeps were collected from γ_0 = 0.1% to 1000% at ω = 1 rad·s^{-1}. At rest and during amplitude sweeps, data was collected at 40 °C and the same **B** field strength as applied during the temperature ramp. Linearity limits were defined as the strain amplitude resulting in a ±5% deviation from the storage modulus in the plateau region (see Sec. SI.11). The values of G' and G'' in this linear viscoelastic region were then defined as G'_{LVE} and G''_{LVE} (see Sec. SI.12). Uncertainty for individual trials was taken as the 95% confidence interval of the y-intercept from linear regression fitting. This uncertainty was propagated through triplicate trials (see Sec. SI.12). Note that reported moduli are first harmonics of the Fourier decomposition, as reported from the rheometer.

Results

Reducing uncertainty in polymer solution magnetorheology using new geometry

As aforementioned, PNIPAM dehydration upon temperature elevation leads to formation of mesoglobules which scatter light, and above a critical polymer content, a weak hydrogel subsequently forms. The relationship between these processes, i.e., dehydration determined by heat flow from differential scanning calorimetry, the dynamic moduli (G', G'') from rheology, and transmittance from turbidimetry is illustrated for 10% PNIPAM solutions (M_n = 59 kDa; "P59") upon heating in Fig. 1a (0.2 °C/min, 0 T). In the absence of **B** field, 10% PNIPAM solutions begin to absorb heat around 30.6 °C (Fig. 1a, red), corresponding to liberation of PNIPAM-water hydrogen bonds (H-bonds) and the onset of polymer dehydration. At slightly higher temperatures ($T_{on,rheo}$ = 31.4 °C), additional dehydration leads to aggregation and the onset of physical hydrogel formation, denoted by an increase in the dynamic moduli (Fig. 1a, black) and a loss factor, $\tan\delta = G''/G'$, of less than unity (Figs. S35, S36).

Shortly thereafter (T_{CP} ~31.8 °C), the system undergoes a transparent-to-cloudy optical transition (Fig. 1a, blue), indicating that PNIPAM chains aggregate into globules sufficiently large to scatter light. Further dehydration upon temperature elevation leads to formation of PNIPAM-rich mesoglobules that form an inter-connected network (Balu et al. 2007; Halperin et al. 2015; Neal et al. 2023b). The increase in the storage and loss moduli of 10% P59 (Fig. 1a)

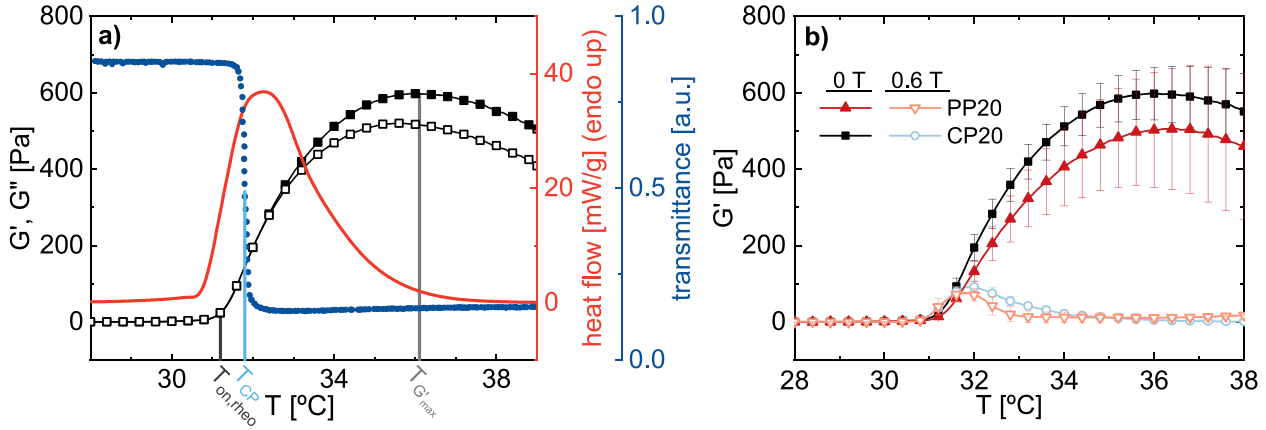

Fig. 1 (a) Storage (G', ■) and loss (G'', □) moduli, heat flow (red solid), and transmittance (blue dotted) of 10% P59 solutions as a function of temperature. G' and G'' collected with CP20 (γ_0 = 0.1%, ω=1 rad·s^{-1}, 0.2 °C/min). (b) G' vs. T for 10% P59 collected with CP20 (squares; same as in (a) but with error bars) or PP20 (triangles, 0.5 mm gap), at 0 T (filled) or 0.6 T (open)

thus corresponds to formation and strengthening of this weak physical hydrogel. The storage modulus then peaks (G'_{max} = 614 Pa) at a temperature, $T_{G'_{max}}$, of 36.5 ± 1.0 °C (Table 1). Beyond this temperature, moduli decay indicates a weakening of the physical hydrogel network. This decay is largely attributed to weakened interactions between nearby mesoglobules due to temperature elevation and worsening solvent quality, resulting in a breakdown of stabilizing attractive interactions (Tanaka 1992, 1993; Balu et al. 2007). Here, this decrease in modulus with further dehydration implies that the continued reduction in mesoglobule pervaded volume due to water liberation leads to a reduction in mesoglobule connectivity (Neal et al. 2023a). Additionally, a small but positive excess volume results as this water is liberated (Niebuur et al. 2019b; Kujawa et al. 2006; Kogure et al. 2005); thus this small increase in solution volume may further reduce connectivity.

Previously, we reported changes in the hydrogel modulus upon temperature elevation when a 0.4 T magnetic field was applied to 10% 87 kDa PNIPAM ("P87") solutions (Neal et al. 2023a). Using a 20 mm parallel-plate ("PP20") geometry, we found that 10% P87 solutions both with and without applied field aggregated into physical hydrogels upon temperature elevation via a two-step process, with the second step leading to a strong physical hydrogel. However, reproducibility between trials utilizing the PP20 geometry was poor, resulting in large error bars — which made determining differences in the rheological behavior due to magnetization challenging. These reproducibility issues are likely due to the low viscosity of semi-dilute PNIPAM, which results in significant spreading during loading.

These issues were abated by employing a new MRD-compatible titanium 20 mm cone-and-plate geometry ("CP20") developed with Anton Paar, enabling magnetic field-dependent changes in PNIPAM hydrogel formation to be detected. Using this CP20 geometry significantly improves the reproducibility of oscillatory temperature ramps on 10% P59 solutions between trials vs. those recorded using the PP20 at a 0.5 mm operating gap (Fig. 1b). While the data from both geometries in Fig. 1b is identical within statistical certainty, the error bars are substantially larger for the PP20 data. In fact at all relevant gap sizes (200–1000 μm), the reproducibility of temperature ramps using the PP20 is worse than that of those using the CP20 (Figs. 2a, S37). The reproducibility of PP20 trials is worse for larger gap sizes (Fig. S37), likely due to significant spreading and incomplete contact between the sample and geometry resulting from higher required sample volumes in the PP20. Beyond increasing the trial-to-trial variability, this spreading leads to a substantial underestimation of G' when compared to the data recorded in the CP20 or at smaller gap sizes in the PP20. Thus, the CP20 was chosen as the measuring system for all remaining trials to minimize the operating gap and sample volume while avoiding measuring artifacts and reproducibility issues.

Despite the lower data quality from PP20 trials, applying a 0.6 T **B** field to 10% P59 during heating leads to a significantly weakened physical hydrogel relative to non-magnetized P59 — whether the CP20 or PP20 (0.5 mm gap) is used. In either geometry, the storage modulus of 10% P59 under 0.6 T increases from about 31 °C to 32 °C before subsequently decaying at higher temperatures (Fig. 1b). In either geometry, the decay in G' at 0.6 T begins at a lower temperature and magnitude than in the non-magnetized equivalent (open vs. closed symbols in Fig. 1b), resulting in a weaker physical hydrogel across the measured temperature range. To better characterize this **B** field weakening of the PNIPAM physical hydrogel, additional field intensities, magnetization times, polymer concentrations, and polymer molecular weights were subsequently examined, all using the CP20 geometry.

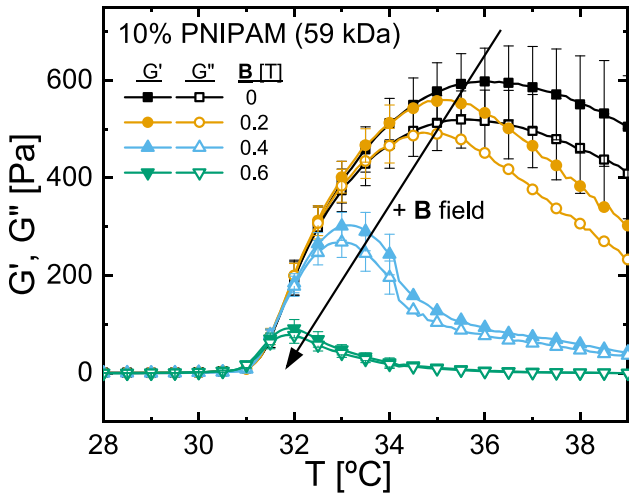

Fig. 2 Storage (filled) and loss (open) moduli as a function of temperature for 10% P59 under varying **B** field intensities (CP20, $\gamma_0 = 0.1\%$, ω=1 rad·s^{-1}, 0.2 °C/min). Error bars are the standard deviation over multiple trials

Table 1 Rheological onset ($T_{on,rheo}$) and maximum storage modulus ($T_{G'_{max}}$) temperatures and maximum storage modulus (G'_{max}) for 10% P59 as a function of **B** field intensity

B field [T]	$T_{on,rheo}$ [ºC]	$T_{G'_{max}}$ [ºC]	G'_{max} [Pa]
0	31.4 ± 0.1	36.5 ± 1.0	617 ± 70
0.1	31.4 ± 0.1	36.8 ± 1.4	640 ± 60
0.2	31.3 ± 0.1	35.4 ± 1.1	576 ± 13
0.3	31.3 ± 0.1	34.2 ± 0.5	449 ± 44
0.4	31.2 ± 0.1	33.2 ± 0.2	308 ± 29
0.5	31.2 ± 0.1	32.7 ± 0.4	229 ± 7
0.6	30.9 ± 0.1	31.9 ± 0.1	93 ± 18

Role of field intensity on hydrogel formation

Oscillatory temperature ramps on semi-dilute, 10% P59 at additional **B** field intensities demonstrate that the maximum hydrogel storage modulus decreases with increasing **B** field intensity (Fig. 2). Applying a **B** field of 0.2 T decreases both the maximum storage modulus G'_{max} and the temperature at which this modulus is achieved vs. the 0 T case (Fig. 2; Table 1). Here, G' and G'' increase with temperature elevation and are nearly identical to those at 0 T just beyond the transition onset temperature. However around 34.5 °C, a noticeable deviation occurs between the moduli at 0 T and 0.2 T. Additionally, the weakly magnetized solutions at 0.2 T reach a G'_{max} of 576 ± 13 Pa at ~35.4 °C. This maximum modulus is 10% weaker compared to the peak modulus of 0 T systems, and occurs at a temperature that is 0.6 °C lower than for the 0 T system (Fig. 2, Table 1).

This weakening of G'_{max} and the shift towards lower temperatures continues with increasing **B** field strength. At the maximum field strength of 0.6 T, G'_{max} for 10% P59 decreases by nearly 85% vs. its value at zero field, with G'_{max} = 93 ± 18 Pa. Additionally, this maximum modulus occurs at a temperature $T_{G'_{max}}$ of 31.9 °C, a 4.6 °C decrease in $T_{G'_{max}}$ vs. at zero field. While 0.1 T magnetic fields do not significantly change either G'_{max} or $T_{G'_{max}}$ compared to the 0 T case (Fig. 3), at higher field intensities, the decrease in G'_{max} and $T_{G'_{max}}$ appears linear. Here, G'_{max} decreases by 1128 ± 89 Pa/T, and $T_{G'_{max}}$ decreases by 9.4 ± 1.8 °C/T above 0.1 T. Extrapolating the former relationship between G'_{max} and **B** forward suggests that a **B** field around 0.69 T would lead to a maximum modulus equivalent to the pre-gelation moduli, implying that no thermal gelation transition would occur at this field strength. However due to instrument limits, studies at higher **B** field could not be conducted.

Interestingly, the 10% P59 solutions display rheological behavior independent of **B** field intensity at the onset of the rheological transition, where the dynamic moduli nearly perfectly overlay just above $T_{on,rheo}$ (Fig. 2). This near-perfect agreement between G' and G'' with increasing **B** appears

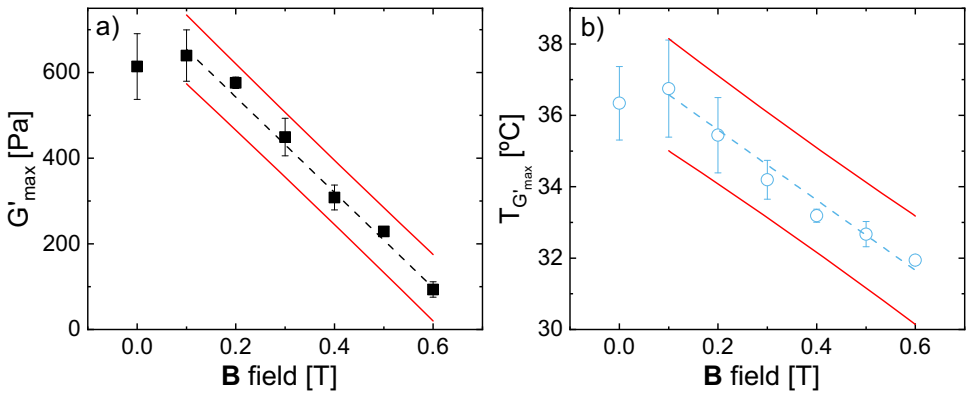

Fig. 3 (a) Maximum storage modulus (G'_{max}) and (b) temperature at G'_{max} ($T_{G'_{max}}$) during oscillatory temperature ramps vs. **B** field for 10% P59. Linear regressions (dashed lines) are fit from 0.1-–0.6 T, shown with 95% confidence intervals (solid lines)

to extend through the temperatures at which the optical transition occurs, corresponding to the formation of PNIPAM aggregates sufficiently large to scatter light; note that a minor decrease in the cloud point transition temperature is expected with increasing **B** (Neal et al. 2023a). Prior work on a higher PNIPAM M_n (87 kDa) showed negligible change in the onset temperature of the DSC transition with increasing field strength, and the measured phase separation enthalpy, ΔH_{sep}, was shown to be independent of field strength above 6% (w/w) PNIPAM (Neal et al. 2023a). Similarly, here pre-magnetization of 10% P59 solutions (0.25 T for 3 days) did not appreciably change ΔH_{sep} (Sec. SI.16). Thus paired with evidence from prior work, this similarity in rheological behavior near $T_{on,rheo}$ and lack of change in ΔH_{sep} suggests that **B** fields do not significantly impact the initial stages of the PNIPAM dehydration and aggregation process — though later stages of this multi-step process could be altered (Niebuur et al. 2019a; Meier-Koll et al. 2012).

However, **B** fields do appear to restrict the ability of PNIPAM aggregates to form strong mesoglobule networks with significant inter-mesoglobule "bonds," thereby hindering the formation of the physical hydrogel that increases G' upon temperature elevation. This idea is supported both by the fact that $G'_{\max}$ continually decreases with increasing field strength and that the temperature at which this maximum modulus occurs concomitantly decreases — meaning that the field-dependent dynamic moduli do not converge at high temperatures, even when normalized by $G'_{\max}$ (Fig. S40). This non-convergence at temperatures corresponding to mesoglobule formation and network development suggests that **B** fields both alter how these processes proceed and narrow the temperature range over which these processes occur. Thus, the **B** field weakening of PNIPAM hydrogels likely arises from altered inter-mesoglobule interactions, motivating subsequent sections which explore how **B** field effects persist when varying other factors known to impact mesoglobule formation (Wu et al. 2004; Gorelov et al. 1997; Niebuur et al. 2019a) such as magnetization time ("Time-dependent magnetic field effects"), and polymer concentration ("Impact of polymer concentration on hydrogel formation in **B** fields") and molecular weight ("Influence of molecular weight on magnetorheology").

Time-dependent magnetic field effects

As the size of PNIPAM mesoglobules formed upon temperature elevation is known to depend on both temperature and temperature ramp rate, dT/dt (Gorelov et al. 1997; Balu et al. 2007), the temperature ramp rate during magnetorheology was next altered to gain more insights into how **B** fields alter mesoglobule and network formation. At zero field, heating PNIPAM solutions more quickly minorly increases both the onset of the rheological transition and the temperature at which the strongest hydrogel forms, $T_{G'_{\max}}$ (Fig. 4a). These increases are consistent with increases in the associated optical transition temperatures observed with increasing temperature ramp rate in both laser light scattering (Shangguan et al. 2014) and turbidimetry (Osváth and Iván 2017), reflecting that PNIPAM chain dehydration and subsequent chain reorganization and aggregation are fairly slow dynamic processes (Shangguan et al. 2014; Osváth and Iván 2017). Just as the clouding transition is a dynamic process, the formation of the PNIPAM physical hydrogel network also takes time; as a result, $T_{G'_{\max}}$ increases as dT/dt increases.

The increase in $T_{G'_{\max}}$ with dT/dt is roughly linear (Fig. 5a, blue squares), consistent with the linear relationship between dT/dt and optical transition onset temperature,

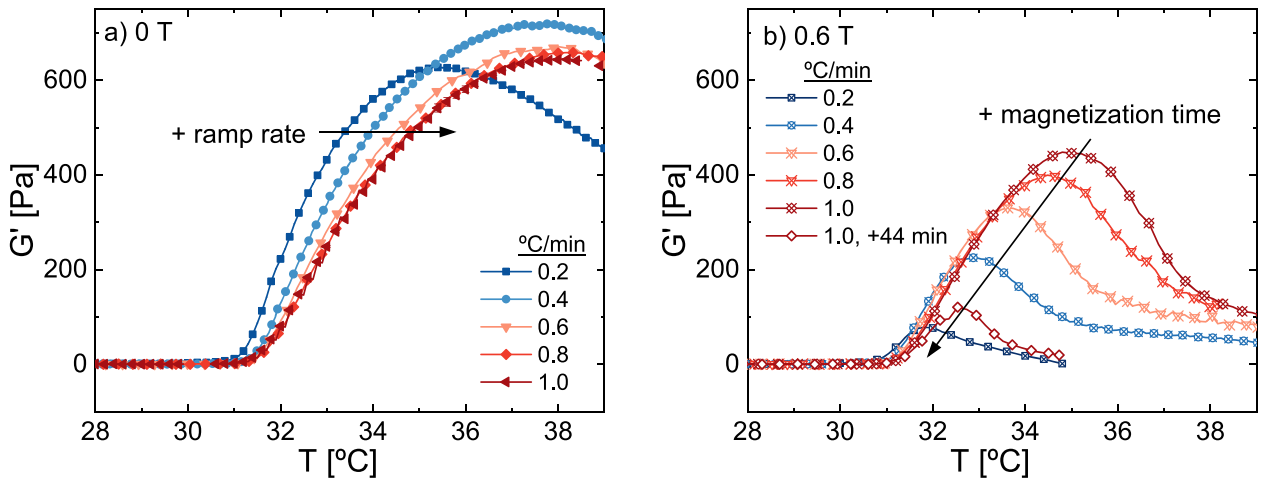

Fig. 4 Storage modulus G' vs. temperature for 10% P59 at temperature ramp rates from 0.2 °C/min to 1.0 °C/min with (a) no **B** field applied (0 T) and (b) 0.6 T field applied. Collected on 20 mm cone-and-plate with $\gamma_0 = 0.1\%$, ω=1 rad·s^{-1}

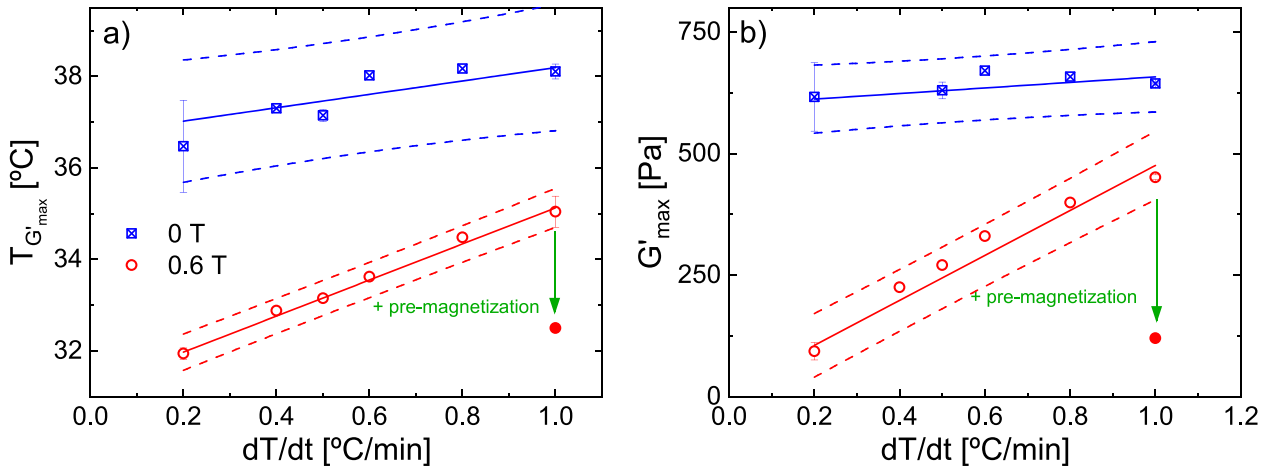

Fig. 5 (a) Temperature of maximum storage modulus during temperature ramps ($T_{G'_{max}}$) and (b) corresponding maximum storage modulus (G'_{max}) as a function of temperature ramp rate (dT/dt) for 10% P59 at 0 T (blue squares) and 0.6 T (red circles). 95% prediction bands are in solid lines, assuming linear regressions. When pre-magnetized at 0.6 T for 44 min prior to 1.0 °C/min temperature ramp, both $T_{G'_{max}}$ and G'_{max} decrease to values near those resulting at 0.2 °C/min

T_{CP}, in turbidimetry measurements of others (Osváth and Iván 2017) and in this system (SI.18). Here, T_{CP} increases linearly with temperature ramp rate at a rate of 3.1 °C per °C/min — similar to that for $T_{G'_{max}}$ (2.9 °C per °C/min). Conversely, G'_{max} at zero field is relatively unaffected by temperature ramp rate (Fig. 5b, blue), and a similar strength hydrogel forms for all temperature ramp rates.

In contrast, both G'_{max} and $T_{G'_{max}}$ strongly increase with increasing dT/dt under 0.6 T magnetic field (Figs. 4b, 5), suggesting a potential antagonistic effect between dT/dt and **B** field. Here, **B** field reduces $T_{G'_{max}}$ and G'_{max} less relative to the 0 T case when the temperature ramp rate is faster (B = 0.6 T, red circles, Fig. 5). For example, when 0.6 T is applied to 10% P59, G'_{max} is reduced by 85% at a ramp rate of 0.2 °C/min vs. the 0 T control, but only reduced by 30% when dT/dt is 1 °C/min (Fig. 5a). This increase in G'_{max} scales linearly with temperature ramp rate, at a rate of 463 ± 59 Pa/ (°C/min); $T_{G'_{max}}$ also increases linearly, by 3.9 ± 0.4 °C/ (°C/min). In other words, as the temperature increases more rapidly and the hydrogel has less time to form due to diffusion limitations, the power of **B** fields to reduce the strength of the physical hydrogel (or the temperature at which G'_{max} occurs) appears to diminish. This finding is in contrast to the zero field case, where only $T_{G'_{max}}$ is dependent on dT/dt.

One potentially important difference between trials at different dT/dt is that trials at higher dT/dt are exposed to the **B** field for less time. Thus while dT/dt and **B** field could act antagonistically, another possible explanation for the trends in Fig. 5 is that this reduced magnetization time reduces the impact of the field on hydrogel microstructure. To test this hypothesis, 10% P59 was "pre-magnetized" at 0.6 T (44 min at 20 °C) prior to performing the oscillatory temperature ramp at 1 °C/min and 0.6 T. Here, both $T_{G'_{max}}$ and G'_{max} shift downward to nearly identical values as those achieved under a slower 0.2 °C/min ramp (Figs. 4b, 5). Note that the 44 min pre-magnetization was chosen such that G'_{max} would occur at roughly the same magnetization time in this 1 °C/min trial as in the 0.2 °C/min trial without pre-magnetization (see Sec. SI.19).

These results suggest that the magnetic field-induced weakening of 10% P59 hydrogels depends more on total magnetization time rather than the temperature ramp rate during hydrogel formation. At higher dT/dt, P59 solutions spend less time exposed to magnetic fields, leading to a decreased weakening effect — which can be recovered if the solutions are simply pre-magnetized before applying a high ramp rate. Similar time-dependent magnetization effects have been reported previously in water (Sronsri et al. 2021), where significant changes in the highest-intensity water peak of the infrared spectra required sufficiently long magnetization times. On this basis, the P59 solutions here likely require some minimum magnetization time (for a given **B** field intensity) for hydrogel strength effects to saturate. Given $T_{G'_{max}}$ and G'_{max} depend on magnetization time for all temperature ramp rates in Fig. 5, magnetic effects do not appear to saturate at these dT/dt.

Although this hydrogel weakening seems to mainly rely on magnetization time, magnetic field application and temperature ramp rate may act individually or in tandem to alter the hydrogel modulus. PNIPAM mesoglobule size is known to strongly depend on thermal history. For example, as previously reported using light scattering (Wu et al. 2004; Gorelov et al. 1997; Niebuur et al. 2019a), increasing dT/dt or quench temperature results in smaller PNIPAM mesoglobules sizes — which could explain to the changes in zero field properties shown in Fig. 5. Similarly, magnetic fields may reduce

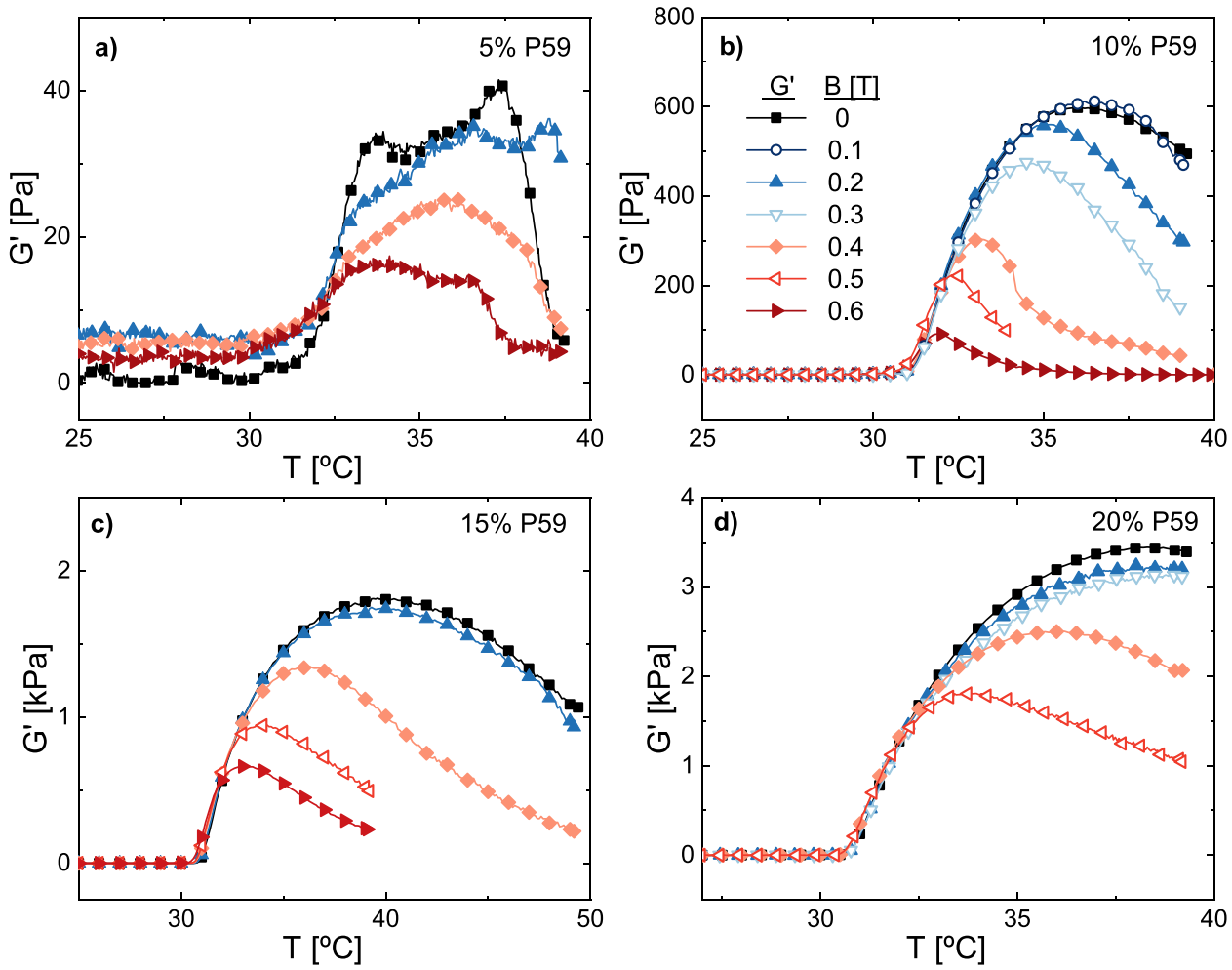

Fig. 6 Storage modulus, G', with increasing temperature as function of **B** field intensity for (a) 5%, (b) 10%, (c) 15%, and (d) 20% P59. (c) is shown up to 50 °C, whereas (d) is shown starting at 27 °C, both for visualization. Significant noise in (a) likely results from low torque near the detection limit

the size of PNIPAM mesoglobules in dilute solutions — though whether this effect is observed depends on thermal history (Sec. SI.20). While dilute solution behavior may not be indicative of field-induced changes at higher P59 content, thermal history and magnetization may nevertheless act in a complex manner to alter hydrogel formation.

Impact of polymer concentration on hydrogel formation in B fields

For solution concentrations between 5% and 20% P59, application of **B** field intensities up to 0.6 T generally decreases the storage modulus at elevated temperatures relative to the equivalent non-magnetized solution (Fig. 6); however, the rheological behavior immediately following the onset of rheological transition is nearly identical for both magnetized and non-magnetized solutions. Similar to that observed in 10% P59, both the maximum modulus and the temperature at which $G'_{\max}$ occurs decrease with increasing field intensity. However interestingly, the critical field intensity required to observe a significant reduction in $G'_{\max}$ and $T_{G'_{\max}}$ appears to increase with increasing concentration. For example, while the oscillatory temperature ramps for 10% P59 are statistically identical at 0 T and 0.1 T (Fig. 6b), nearly identical responses with increasing temperature are observed up to 0.3 T for 20% P59 (Fig. 6d). Nevertheless, in 5%-20% P59 solutions, the resulting volume fraction of PNIPAM-rich mesoglobules is sufficient to form a weak physical hydrogel above $T_{on,rheo}$.

The similarity in the rheological behavior across P59 concentrations and **B** field intensities is attributed to the similar concentration regime for these solutions. Each of these P59 solutions is above the P59 overlap (c^*) concentration at 25 °C, but is below the cross-over concentration (c^{**}) at 25 °C. The overlap concentration boundary is often estimated

as $1/[\eta]$ (Bohidar 2015), where $[\eta]$ is the molecular weight-dependent intrinsic viscosity. For P59, the intrinsic viscosity at 25 °C is approximately 48 mL/g as measured via dynamic light scattering (Sec. SI.5) and confirmed via rheology (Sec. SI.6). Thus, $c^*_{P59} \sim$ 2.1% (w/w) at 25 °C. However, the PNIPAM chain radius of gyration is reduced slightly with increasing temperature even prior to the LCST (Wu and Zhou 1996; Wang et al. 1998; Wu and Wang 1998; Wang and Wu 1999) and the chain and mesoglobule pervaded volume both decrease upon temperature elevation as water is liberated (Tavagnacco et al. 2018; Krasovitski et al. 2004), leading to a loss in network connectivity and a decrease in G' at temperatures above $G'_{\max}$ (Neal et al. 2023a). As such, these concentration regime values should be regarded as estimates only. Given that all P59 concentrations here are above c^* at 25 °C, qualitative similarity in their responses to **B** fields may be due to their similarity in concentration regime; note that no hydrogel is expected to form in dilute and non-interacting systems ($c < c^*$) and that jammed, thoroughly entangled systems may exhibit significant differences due to entanglement effects ($c > c^{**}$).

At 5% P59, the polymer concentration is only twice that of c^* at 25 °C, resulting in a weak physical gel with a $G'_{\max}$ around 40 Pa at 0 T (Fig. 6a). Compared to the 10% P59 solution at 0 T, this $G'_{\max}$ is more than an order of magnitude lower (~40 Pa vs. 614 Pa) due to the reduced polymer content. The zero-field, 5% P59 solutions also begin the rheological transition ($T_{on,rheo}$) at a higher temperature than 10% P59 solutions (31.7 °C vs. 31.4 °C, respectively; Table S5). For all P59 concentrations herein, $T_{on,rheo}$ decreases with increasing P59 content (to 29.7 °C at 20% P59), indicating that 20% P59 is likely below or near the critical volume fraction ϕ_c corresponding to the minimum lower-critical solution temperature on the T vs. ϕ phase diagram. As PNIPAM concentration increases, local concentration fluctuations cause more frequent nucleation of PNIPAM-rich areas, promoting the phase transition at lower temperatures (Yanase et al. 2020).

Similar to 10% P59 (Fig. 6b), increasing **B** decreases $G'_{\max}$ of 5% P59 from ~40 Pa at 0 T to ~18 Pa at 0.6 T. The temperature of the maximum modulus $T_{G'_{\max}}$ is also reduced by **B** application; however, these changes are only qualitatively compared due to the low signal from the weak 5% P59 materials. At this lower concentration, the P59 solution forms only a weak aggregate network and is far below c^{**} (Sec. SI.6) at 25 °C, denoting a lack of extensive entanglements. While entanglements may form during initial collapse in semi-dilute PNIPAM, their disentanglement is relatively rapid and unconstrained (Yushmanov et al. 2006; Lu et al. 2011).

At 15% and 20% P59, the polymer concentration is sufficient to form stronger physical hydrogels, with $G'_{\max}$ at zero field around 1.8 kPa and 3.2 kPa, respectively (Fig. 6c, d). However, increasing **B** field intensity still decreases G' of 15% and 20% P59 at elevated temperatures relative to the 0 T case following the initial hydrogel formation region ($T > T_{on,rheo} + 2$ °C). Interestingly, in contrast to both 5% and 10% P59, the storage modulus of both 15% and 20% P59 solutions at 0 T increases with increasing temperature to much higher $T_{G'_{\max}}$ (≈ 40 °C). Unlike at lower P59 concentrations where the tail of the DSC curve coincides with $T_{G'_{\max}}$ (Fig. 1a), this water liberation stage occurs prior to $T_{G'_{\max}}$ in 15% and 20% P59 solutions (Fig. S46) — meaning that the loss in network connectivity occurs well beyond completion of polymer dehydration. Prior studies have noted that at higher concentrations, liberated water can become trapped in pockets within the forming PNIPAM mesoglobule due to the presence of a dense PNIPAM shell, which slowly escapes in time (Niebuur et al. 2019b; Philipp et al. 2014; Ramon et al. 2001). Thus this temperature mismatch between the end of polymer dehydration and when $G'_{\max}$ occurs is likely because the mesoglobules retain larger volumes after dehydration due to this trapped water, thereby maintaining network connectivity.

Interestingly, while a 0.2 T field dramatically alters the rheological response in 10% P59 (Fig. 6b), a much less substantial change in response is observed at 0.2 T for the 15% and 20% P59 solutions (Fig. 6c, d). In general, the minimum field intensity required for $G'_{\max}$ to decrease appears to increase with increasing polymer content (Figs. 6, S47). This effect persists at higher field intensities, suggesting that the ability of the field to lower $G'_{\max}$ depends on polymer content (Fig. S47), with the field exhibiting less of an effect at higher polymer content. This finding is consistent with our prior work showing that **B** fields altered ΔH_{sep} less at higher polymer contents. One possible explanation is that although all P59 solutions are below c^{**} at 25 °C (Sec. SI.7), additional stabilizing physical linkages or entanglements between PNIPAM mesoglobules are more likely at higher polymer contents, potentially reducing the ability of the **B** field to weaken the hydrogel. Interestingly, despite the reduced ability to weaken $G'_{\max}$ at higher polymer content, applied **B** fields actually reduce $T_{G'_{\max}}$ more at higher polymer concentrations (Sec. SI.23). The possible origins of this apparent discrepancy will be examined further in "Discussion".

Influence of molecular weight on magnetorheology

Magnetically induced weakening of PNIPAM physical hydrogels persists in PNIPAM solutions with nearly twice (108 kDa, "P108," Fig. 7a) and half (30 kDa, "P30," Fig. 7b) the number-average molecular weight (M_n) as P59. At zero field, the onset of rheological transition for 15% PNIPAM solutions, $T_{on,rheo}$, is actually the lowest for P30 (30.0 °C) but

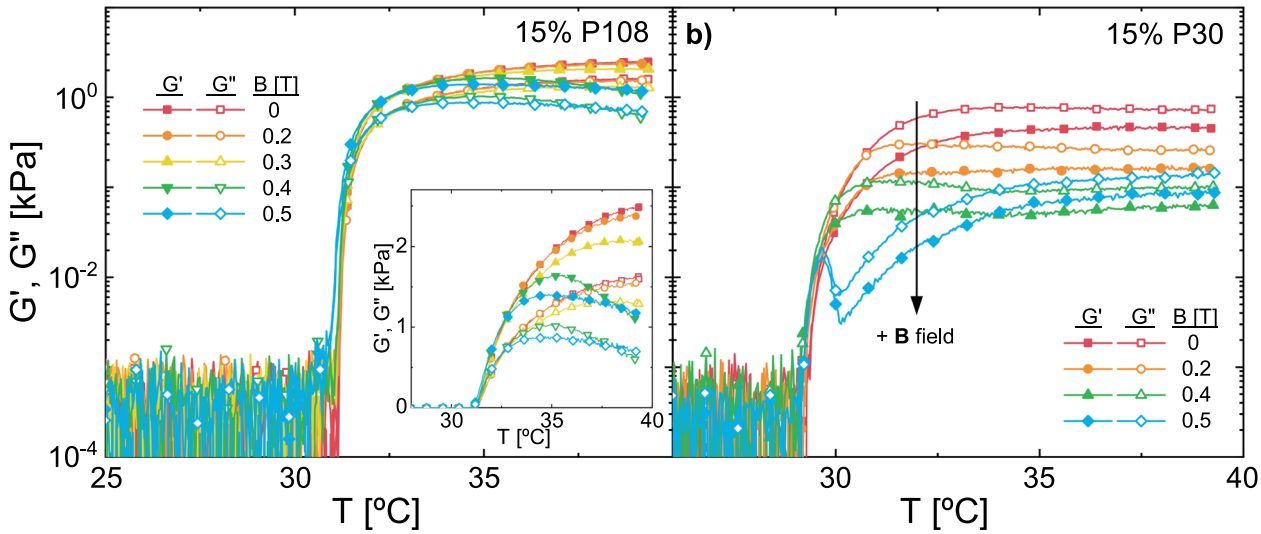

Fig. 7 Storage modulus, G', with increasing temperature as function of **B** field intensity for aqueous 15% (a) P108 and (b) P30

increases to 31.2 °C and 31.4 °C for P59 and P108 solutions, respectively (Table 2). While optical and rheological phase transition onset temperatures typically *decrease* with increasing PNIPAM molecular weight (Qiu et al. 2013), end group effects may alter or reverse this relation (Tong et al. 1999; Ru and Feng 2011; Qiu et al. 2013). Alternatively, the reported rheological onset temperatures, $T_{on,rheo}$, may be artificially shifted with changes in molecular weight due to differences in the rheological behavior and mechanisms underlying the increase in modulus at elevated temperatures. Both P59 and P108 form "hydrogels" upon temperature elevation, where the storage modulus exceeds the loss modulus at all temperatures above $T_{on,rheo}$ for all field intensities (Figs. 6c, 7a) and for much of the frequency-dependent relaxation spectrum at 40 °C (Secs. SI.13, SI.32). Conversely, 15% P30 remains a viscoelastic liquid under all conditions, exhibiting G'' greater than G' at all temperatures above $T_{on,rheo}$ (Fig. 7b) and across the frequency spectrum at 40 °C (Fig. S49).

Similar to 15% P59 solutions, the storage moduli increase for both 15% P108 and 15% P30 solutions for roughly 10 °C following $T_{on,rheo}$ at 0 T (Fig. 7a and b, respectively). However, the temperature range over which this increase in dynamic moduli occurs ($T_{on,rheo} < T < T_{G'_{max}}$) also increases with increasing M_n, from 7.9 °C in P30 to 8.9 °C in P59 and 10.7 °C in P108. As mesoglobule formation and formation of the hydrogel is a diffusion-limited process (Van Durme et al. 2004; Papadakis et al. 2024; Osváth and Iván 2017; Shangguan et al. 2014), this increase in temperature range from the transition onset to the maximum hydrogel strength ($\Delta T_{rheo} = T_{G'_{max}} - T_{on,rheo}$) is potentially due to slower diffusion of forming mesoglobules in high molecular weight solutions. In other words, the modulus of higher molecular weight PNIPAM solutions is higher following $T_{on,rheo}$ (Fig. S50), which slows the movement of mesoglobules and broadens the rheological transition. Further, the loss factor at the peak modulus, tan δ_{max}, decreases with increasing polymer molecular weight (Table 2) — suggesting that increased physical interactions and entanglements between mesoglobules at higher M_n create a more solid-like network.

Table 2 Rheological onset ($T_{on,rheo}$) and maximum storage modulus ($T_{G'_{max}}$) temperatures, maximum storage modulus (G'_{max}), and loss factor at maximum storage modulus ($tan\ \delta_{max}$) for 15% PNIPAM solutions as a function of polymer molecular weight (M_n) formed under 0 T

M_n [kDa]	$T_{on,rheo}$ [°C]	$T_{G'_{max}}$ [°C]	G'_{max} [Pa]	$tan\ \delta_{max}$ [1]
30	30.0	37.1	470	1.58
59	31.2	39.5	1810	0.87
108	31.4	42.0	2500	0.65

As in P59, increasing the magnetic field intensity decreases both G'_{max} and $T_{G'_{max}}$ in 15% P108 (Fig. 7a) and 15% P30 (Fig. 7b). Similar to the trends observed with increasing polymer content, **B** fields appear to reduce G'_{max} less at higher M_n (Fig. 7a vs. b; Fig. S51), again suggesting that physical interactions between mesoglobules may help stabilize the hydrogel and prevent **B**-induced weakening. Interestingly, the shift in $T_{G'_{max}}$ with **B** fields is notably more pronounced in P108 than in P59 (−6.6 °C vs. −3.8 °C from 0 T to 0.4 T, respectively), leading to a smaller ΔT_{rheo} in P108 at higher fields. Although in the absence of magnetic fields, P108 undergoes a broader rheological transition, the polymer dehydration process occurs over a more narrow temperature range in P108 than in P59 (3.9 °C vs. 4.4 °C; Fig. S52, Table S6), likely due to the lower dispersity of P108. Here, the polymer dehydration range width is defined as the temperature range between the onset of heat flow, $T_{on,DSC}$,

and the temperature of 95% of the total phase transition enthalpy, $0.95\Delta H_{sep}$ (Sec. SI.27). As **B** fields are known to alter solvent polarization and PNIPAM hydrophobic hydration (Neal et al. 2023a; Sronsri et al. 2021; Pang 2006; Pang and Deng 2008a), the PNIPAM dehydration and mesoglobule formation process during magnetization may occur more completely over a smaller temperature range in P108 than in P59, causing this reduction in ΔT_{rheo} in P108.

As aforementioned, across the entire rheological transition regime ($T > T_{on,rheo}$) and all magnetic fields examined herein, 15% P30 solutions behave as viscoelastic liquids, with tan $\delta > 1$ — unlike 15% P59 and P108 which behave as viscoelastic hydrogels with tan $\delta < 1$. Amplitude sweeps confirm that the applied deformation is linear (Fig. S53), and frequency sweeps confirm $G'' > G'$ across all frequencies probed (Fig. S49). According to mode-coupling theory (MCT) (Mason and Weitz 1995), at sufficiently high volume fraction and inter-particle attractions, particles in a suspension will become kinetically trapped into an attractive-driven glass (ADG). However here, we propose that P30 solutions form mesoglobules with inter-particle attractions at elevated temperatures, but these interactions and the polymer concentration are insufficient to induce formation of a physical hydrogel. This difference leads to distinct rheological behavior in P30 solutions with magnetization. While magnetic fields still weaken both G' and G'' like in P59 and P108, the dynamic moduli generally plateau at elevated temperatures — as opposed to reaching a maximum value and subsequently decaying as network connectivity is lost (Neal et al. 2023a). Additionally, anomalous changes in the magnetic field-induced weakening are observed at 0.5 T compared to lower field strength counterparts (Fig. 7b, blue). While the temperature at which $G'_{\max}$ occurs generally decreases with increasing **B**, the moduli peak, decay, and then rise again at 0.5 T. This peculiar behavior intensifies at 0.6 T (Figs. S55, S56). Although unusual, the differences in rheological behavior upon magnetization in P30 are likely due to its viscoelastic liquid-like behavior at all conditions, which is not observed in any other solution.

To further test the hypothesis that increased physical interactions and entanglements between mesoglobules prevent **B** field-induced modulus weakening, the rheological behavior of a higher molecular weight (M_n = 314 kDa, P314) and high dispersity ($Đ$~ 3.03) PNIPAM was examined. P59 and P108 solutions exhibit a peak in G' and subsequent decay at elevated temperatures, which has previously been attributed to a loss of network connectivity due to a reduction in mesoglobule size upon water expulsion (Neal et al. 2023a). However in 7.5% P314 solutions, G' monotonically increases with temperature (Sec. SI.29). This rheological behavior mirrors that of other entangled PNIPAM solutions, which were hypothesized to maintain connectivity at elevated temperatures due to stability afforded by additional physical linkages between mesoglobules (Neal et al. 2023a, b). Other authors have described this phenomenon as a "pearl-necklace" conformation, where dehydrated PNIPAM-rich pearls are linked by solvated PNIPAM chains (Wang et al. 2022). Perhaps unsurprisingly, in contrast to the behavior observed when $M_n \leq 108$ kDa, P314 is unaffected by the application of a 0.4 T magnetic field. Here, the dynamic moduli of magnetized and non-magnetized 7.5% P314 solutions are statistically identical at all measured temperatures (Fig. S57). Thus, the high polymer dispersity and the presence of MDa-length chains in P314 appear to prevent magnetic fields from reducing the strength of the resulting hydrogel.

Nonlinear rheology of PNIPAM hydrogels formed under B fields

Magnetic fields generally decrease the strength of PNIPAM hydrogels relative to non-magnetized controls in the linear viscoelastic regime (LVE), across molecular weights, concentrations, and temperature ramp rates. Finally, the nonlinear flow behavior of 15% and 20% P59 solutions under applied **B** field was examined to provide additional insight into the mechanisms underlying field-induced changes in microstructure (Fig. 8). Following oscillatory temperature ramps, 15% P59 solutions at 40 °C in the absence of **B** field show viscoelastic solid-like behavior with a loss factor of less than unity (tan δ = 0.86; Table 3). Here the linear viscoelastic (LVE) region extends to an amplitude of ~5% (Fig. 8a); see Fig. S34 for standard deviations on amplitude sweeps from multiple trials. In this LVE region, the physical hydrogel formed from 15% P59 exhibits average G' and G'' values of 1.7 kPa and 1.5 kPa, respectively (Fig. S33; Table 3), signifying a relatively strong physical network. Above 5% strain, the solution begins to shear thin with tan δ exceeding unity at $\gamma_0 \approx 170\%$. Lissajous-Bowditch curves for select relevant strains are shown in Fig. S59, exhibiting a clear transition to nonlinearity by γ_0 = 10%.

Following the onset of nonlinear deformation, a second pseudo-linear plateau is observed (20%< γ_0 <150%) before another region of modulus decay (Fig. 8a). This two-step yielding behavior has been reported previously in a variety of systems and is characteristic of ADGs. Note that these networks would be considered a "glass" or "gel" depending on the volume fraction (Zaccarelli and Poon 2009); however here, the total mesoglobule volume fraction is unknown because the amount of water in each globule is unknown. This two-step yielding typically attributed to the breakup of structures on two separate length scales at different stress limits (Pham et al. 2008; Laurati et al. 2011; Koumakis and Petekidis 2011; Joshi and Tata 2017; Ahuja et al. 2020; Franco et al. 2021). For example, Pham et al. (2008) and Koumakis and Petekidis (2011) found a two-step yielding behavior in an ADG formed from poly(methylmethacrylate)

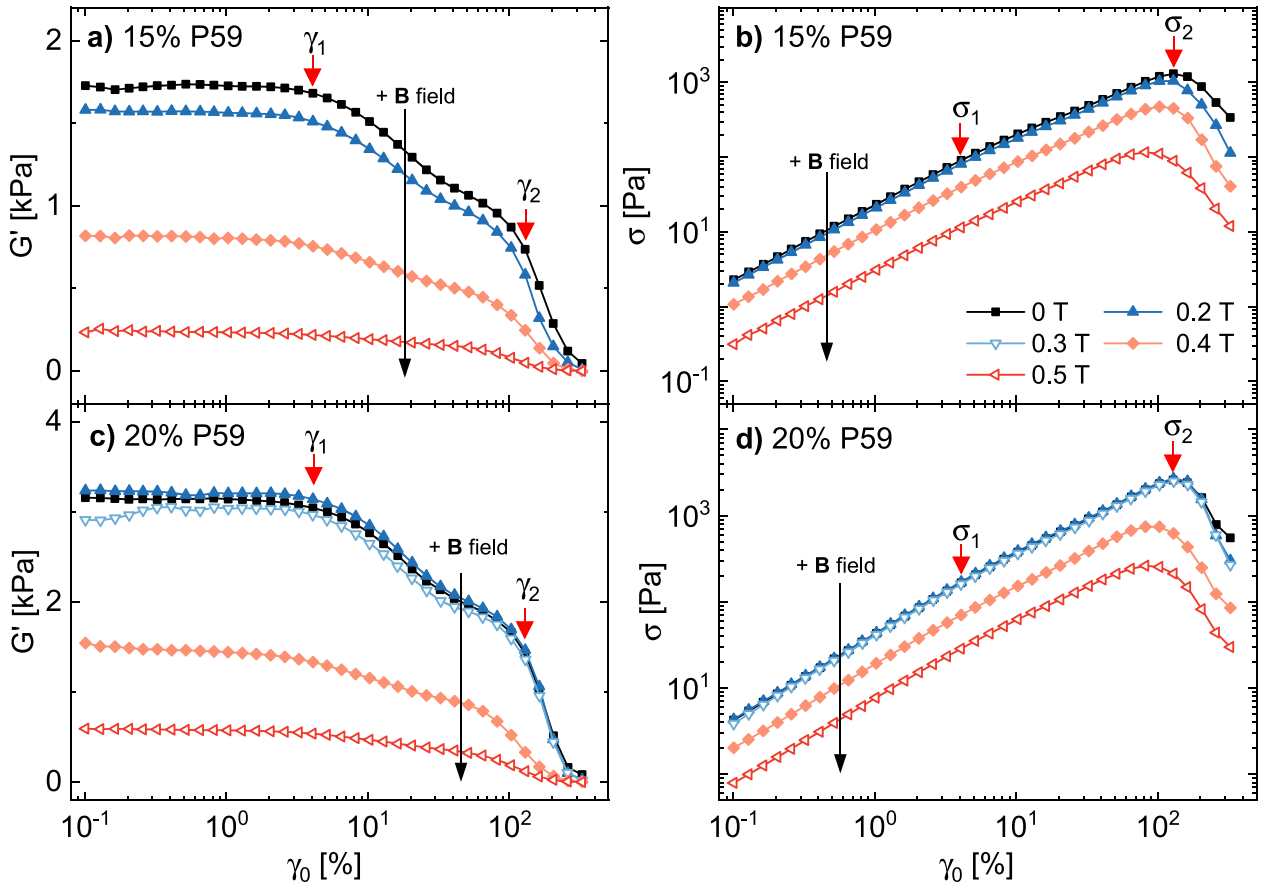

Fig. 8 Amplitude sweeps under applied **B** following oscillatory temperature ramps at same **B** (γ_0 = 0.1%, ω=1 rad·s^{-1}, 0.2 °C/min). (a, c) G' (first harmonic) and (b, d) stress σ as a function of strain amplitude γ_0 for (a, b) 15% and (c, d) 20% P59 at 40 °C

(PMMA) microgels grafted with poly(hydro-stearic acid) (PHSA). The first yielding step (at strain amplitude $\gamma = \gamma_1$) corresponded to the breakup of bonds between PMMA-PHSA clusters, whereas the second yielding step (γ_2) signaled the breakup of clusters into smaller constituents. Similarly, Franco et al. (2021) noted that PNIPAM microgel systems (0.9% (w/w)) contained two steps of shear thinning; the first yielding step (γ_1) was attributed to the disruption of PNIPAM microgel particle-particle interactions whereas the second (γ_2) was attributed to the breakage of nearest-neighbor particle cages, eliminating longer-range correlations and allowing particles to flow. Saisavadas and coworkers (2023) examined the large amplitude oscillatory shear (LAOS) behavior of PNIPAM microgels with and without dangling chains using the sequence of physical processes method (Rogers et al. 2011). This work showed that entanglements between nearby PNIPAM mesoglobules are largely responsible for the first yielding transition (Saisavadas et al. 2023). Both the two-step yielding (Fig. 8) and Lissajous-Bowditch curves across the yielding transition (Fig. S59) for semi-dilute PNIPAM solutions here are qualitatively similar to the entangled PNIPAM microgel systems investigated by Saisavadas et al. (2023). Accordingly, the two-step yielding behavior of semi-dilute PNIPAM seen here is proposed to correspond to the breakage of short-range inter-cluster attractive associations and entanglements between mesoglobules (step 1, $\gamma > \gamma_1$) and the breakage of nearest-neighbor cages allowing mesoglobules to flow ($\gamma > \gamma_2$) as illustrated in Fig. 9.

When formed under the presence of 0.2 T **B** fields, physical hydrogels from 15% P59 weaken to a G'_{LVE} of 1.6 kPa and G''_{LVE} of 1.3 kPa (see Fig. S33; Table 3). Consistent with the oscillatory temperature ramps under applied field (Fig. 6c), the linear dynamic moduli (G'_{LVE}, G''_{LVE}) of 15% P59 hydrogels decrease at 40 °C with increasing field strength. This decrease in G' and G'' is dramatic at higher field strengths, consistent with the peak and rapid decline in moduli at higher temperatures. Consequently, the corresponding stress at each strain amplitude and the linear viscoelastic loss factor, tan δ, also decrease with increasing **B** intensity (Fig. 8b; Table 3).

Based on the proposed yielding mechanism (Fig. 9), the strain corresponding to the first yielding step (γ_1 in Fig. 8a) estimates the strain required to break the short-range inter-

Table 3 Storage modulus (G'_{LVE}) and loss factor (tan δ_{LVE}), strain and stress after first yield step (γ_1, σ_1), and strain and stress at second yield step (γ_2, σ_2) for 15% P59 as a function of **B** intensity, from amplitude sweeps at 40 °C. Reported uncertainty is the standard deviation (n = 3)

B field [T]	G'_{LVE} [Pa]	tan δ_{LVE} [1]	γ_1 [%]	σ_1 [Pa]	γ_2 [%]	σ_2 [Pa]
0	1720 ± 16	0.86 ± 0.01	3.7 ± 0.6	82.4 ± 16.9	146 ± 23	1350 ± 280
0.2	1570 ± 16	0.86 ± 0.01	3.7 ± 0.6	74.6 ± 21.4	116 ± 18	1130 ± 370
0.4	840 ± 13	0.83 ± 0.01	2.9 ± 0.5	31.5 ± 16.4	103 ± 0.1	500 ± 240
0.5	240 ± 8	0.82 ± 0.01	3.3 ± 0.1	9.4 ± 1.5	82 ± 0.1	120 ± 9

particle bonds (Pham et al. 2008). Interestingly, γ_1 does not vary significantly with magnetic field intensity in 15% P59 (3.7% in 0 T vs. 3.3% in 0.5 T, Table 3), suggesting that the length scale associated with the range of inter-particle attractions is not significantly changed by **B** at 40 °C. However, the resulting stress at this first yielding step, σ_1, is an order of magnitude lower at 0.5 T vs. 0 T (Fig. 8b).

While direct connections between neighboring mesoglobules break around 4% strain (γ_1), mesoglobules are prevented from moving freely due to caging interactions until higher strain amplitudes. A schematic for the rearrangement allowed above γ_1 and γ_2 is shown in Fig. 9, showing that large-scale topology only occurs above γ_2. The force required to break nearest-neighbor cages is thus estimated by the peak stress (σ_2) in terms of σ vs. γ_0 (Fig. 8b; see also Fig. S34), at a corresponding strain γ_2. In 15% P59 at zero field, this cage breakup occurs at roughly 146% strain, corresponding to σ_2 = 1.3 kPa (Table 3). Accordingly, mesoglobule cage distortions allow for motion on the order of 146% of the particle diameter (Pham et al. 2008). Under 0.5 T, these values for γ_2 and σ_2 decrease to 82% and 120 Pa, respectively, suggesting that the local motion lengths allowed by particle cages prior to cage breaking decrease upon magnetization. Pham et al. suggest that γ_2 corresponds to the "topology-breaking strain" — an approximation for the length scale of correlated movement by nearby particles (Pham et al. 2008) — suggesting that magnetized systems exhibit a shorter length-scale for correlation. One possible explanation is that magnetization creates tighter cages around each mesoglobule, potentially due to the formation of more, smaller mesoglobules with magnetization (Sec. SI.20). Another likely possibility is that magnetized hydrogels have lower connectivity at 40 °C than those at 0 T, requiring a lower topology-breaking strain to observe widespread flow. This lower connectivity at 40 °C is more pronounced at higher **B**, because 40 °C is further from $T_{G'_{max}}$ at higher field strengths.

Hydrogels formed from 20% P59 (Fig. 8c, d) and 15% P108 (Sec. SI.32) show qualitatively similar changes in nonlinear rheology upon magnetization as 15% P59, with magnetized hydrogels having lower γ_2, σ_1 and σ_2. Due to the higher polymer content, G'_{LVE} for non-magnetized 20% P59 is higher than 15% P59 (3.1 kPa vs. 1.7 kPa, respectively). However, tan δ_{LVE} is ~0.9 at both concentrations. Similarly, γ_1 for non-magnetized 20% P59 is roughly 4% and γ_2 is 130%, only slightly lower than in 15% P59 systems (γ_2 =150%). With a higher polymer concentration, the

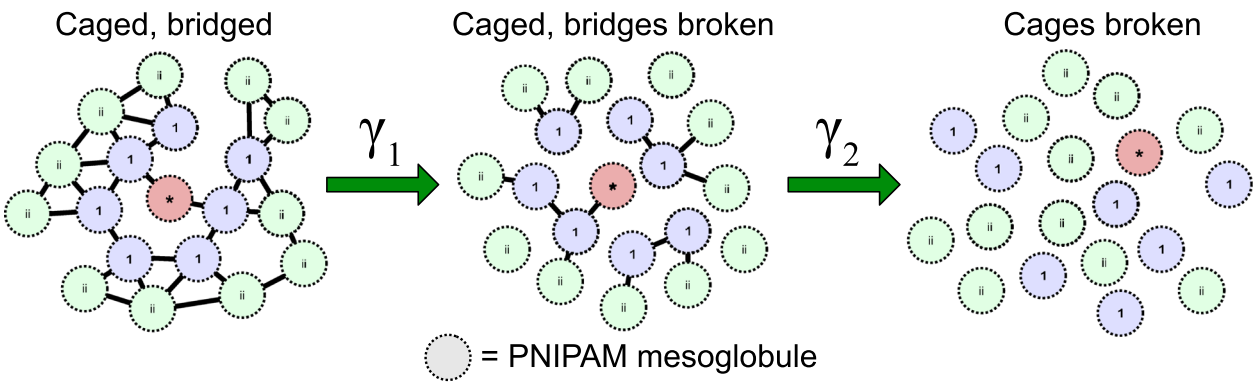

Fig. 9 Networks of PNIPAM-rich mesoglobules in semi-dilute hydrogels yield in two steps. First, attractions between mesoglobules break and reform when $\gamma > \gamma_1$. Widespread network rearrangement occurs when $\gamma > \gamma_2$ due to melting of the network. Mesoglobules colored for visualization by location before strain sweeps as (red, "*") mesoglobule of interest, (blue, "1") direct neighbors and (green, "ii") other mesoglobules. Above γ_1, the relative topology of nearest neighbors remains the same, but bonds between nearest neighbors may break. Above γ_2, widespread flow permits topology to change. Adapted from Pham et al. (2008) and Zhao et al. (2014)

mesoglobule cage size is likely smaller in 20% P59, decreasing γ_2 accordingly. Just as in 15% P59, values of γ_2 and tan δ_{LVE} all decrease with increasing **B** field strength whereas γ_1 remains roughly constant. Thus as the nature of mesoglobule interactions is similar between 15% and 20% P59, the length-scale of deformation to break these bonds is also similar between the two systems ($\gamma_1 \approx 4\%$).

Discussion

Magnetic (**B**) field application clearly alters the rheological response of hydrogels that form in PNIPAM solutions at elevated temperatures — leading to lower maximum moduli and a lower maximum temperature at which G' achieves its maximum value. An outstanding question is how specifically magnetic fields alter the mesoglobule formation and network formation process to decrease both $G'_{\max}$ and $T_{G'_{\max}}$. During magnetization, several common features of the hydrogel formation process are apparent across a range of molecular weights (30–314 kDa) and polymer concentrations (5–20% wt): (1) **B** fields usually weaken the resulting hydrogel modulus at elevated temperature unless M_n is high; (2) G' during the initial rheological transition (corresponding to the initial mesoglobule formation process) appears unchanged with **B** fields; (3) both $G'_{\max}$ and $T_{G'_{\max}}$ decrease with increasing **B**. Given that the polymer concentration does not change during magnetization, the most plausible explanations for this field-induced weakening are either a change to the mesoglobule size and the resulting network connectivity, a change in the interactions between mesoglobules, or some combination of both.

Based on the evidence from experiments and our prior work (Neal et al. 2023a), we propose that because **B** fields alter solvent polarization and solvent quality (Sronsri et al. 2021; Neal et al. 2023a), **B** fields also alter the mesoglobule formation process to weaken the resulting hydrogel. This hypothesis is also consistent with the observation that magnetization time is the most important parameter in determining the hydrogel modulus ("Time-dependent magnetic field effects"), as prior works demonstrate that field-induced changes in solvent properties are strongly time-dependent (Sronsri et al. 2021; Liu and Cao 2021; Cai et al. 2009; Holysz et al. 2007). We previously showed that **B** fields marginally worsen solvent quality and reduce the hydrophobic hydration around the PNIPAM isopropyl groups (Neal et al. 2023a). Hydrophobic hydration is thought to play a crucial role in the aggregation of polymer chains into mesoglobules, and any disruptions or enhancement to hydrophobic hydration can influence the mesoglobule size, density and surface properties (Bischofberger et al. 2014; Bischofberger and Trappe 2015). Specifically, significantly larger mesoglobules are expected when the hydrophobic groups are well hydrated (Niebuur et al. 2019a, b); thus conversely, smaller mesoglobules would be expected when hydrophobic hydration worsens. This reduction in mesoglobule size with magnetization is at least plausible based on DLS measurements in dilute PNIPAM solutions (Sec. SI.20).

A change in mesoglobule size only cannot account for the observed changes in rheological behavior. For example, if **B** fields caused formation of smaller mesoglobules with fewer chains per globule but the mesoglobule composition remained the same (i.e., same ratio of polymer and water), more total mesoglobules would form in solution, leading to a smaller network mesh size and consequently, a stronger — not weaker — hydrogel modulus. However, a change in both the mesoglobule size and composition — specifically that magnetization creates less watery mesoglobules — could account for all of the changes observed with **B** fields, and is also supported by prior work. Increasing the temperature ramp rate or quench depth leads to the formation of smaller, denser mesoglobules with less water (Niebuur et al. 2019a; Balu et al. 2007; Gorelov et al. 1997), because the thermodynamic driving force for phase separation is stronger. Additionally, during the mesoglobule formation process at 0 T, hydrophobic hydration layers surround isolated, dehydrated PNIPAM chains which are thermodynamically driven to cluster into mesoglobules (Tanaka 1993, 1992). Disruption of these hydrophobic hydration layers by **B** fields may thus increase the affinity for PNIPAM mesoglobules to form with lower hydration than non-magnetized mesoglobules. Based on this evidence and that magnetization marginally worsens solvent quality and reduces hydrophobic hydration (Neal et al. 2023a), the mesoglobules formed following magnetization would likely also be less watery.

This proposed change in mesoglobule size and water content is consistent with all of the general observations from the rheology. For example, smaller mesoglobules with less water would lead to a smaller overall mesoglobule volume fraction in solution, reducing the achievable $G'_{\max}$. Additionally, $T_{G'_{\max}}$ would also likely decrease with formation of smaller, less watery mesoglobules, due to the smaller total mesoglobule volume fraction in solution. The fact that solutions with lower polymer content (Fig. 6) exhibit lower $T_{G'_{\max}}$ supports this hypothesis. Additionally, as network formation is a diffusion-limited process (Van Durme et al. 2004; Papadakis et al. 2024; Osváth and Iván 2017; Shangguan et al. 2014), these smaller mesoglobules can diffuse faster than their larger, non-magnetized counterparts — which could also explain the decrease in $T_{G'_{\max}}$ with field intensity. Finally, although higher polymer contents appeared to reduce the ability of **B** fields to lower $G'_{\max}$, the reduction in $T_{G'_{\max}}$ was actually *larger* with higher polymer content (Sec. SI.23). This apparently anomalous trend can also be reconciled by

the formation of smaller, less watery mesoglobules. As aforementioned, complete water liberation occurs prior to $T_{G'_{max}}$ for higher concentration PNIPAM solutions (Fig. S46); this delayed loss of network connectivity likely occurs because at higher polymer contents, some liberated water is trapped within the mesoglobule and the mesoglobule retains a larger size (Niebuur et al. 2019b; Philipp et al. 2014; Ramon et al. 2001). Thus if magnetized mesoglobules form with substantially less water and this water cannot be trapped at higher polymer contents, the difference in $T_{G'_{max}}$ between 0 T and magnetized solutions would increase.

Finally, the suggested alteration in both the size and water content of the magnetized mesoglobules is consistent with the comparable rheological behavior for solutions exposed to varying magnetic field strengths during formation. During the initial stages of the phase transition in PNIPAM solutions at 0 T, mostly solvated PNIPAM chains locally concentrate into proto-mesoglobules (Niebuur et al. 2019a). Here, small angle neutron scattering confirmed that these watery, loosely packed aggregates form initially, regardless of quench depth. These SANS measurements thus support the observation that the initial mesoglobule formation process and initial rheological transition are nearly independent of field application ("Impact of polymer concentration on hydrogel formation in **B** fields").

As is the case for other polymer properties, increasing polymer content (ϕ_p) and increasing molecular weight (M_n) show similar field-induced effects, where **B** fields appear to reduce the hydrogel modulus less at higher polymer content (Fig. S47) or molecular weight (Fig. S51). This reduced weakening effect at higher ϕ_p and M_n supports the hypothesis that **B** fields primarily reduce the total volume fraction of mesoglobules in solution. At higher ϕ_p or M_n, physical stabilizing interactions — including entanglements between mesoglobules or the formation of a "pearl-necklace" structure — are more prevalent (Yanase et al. 2020; Chuang et al. 2000; Wang et al. 2022). As a result, this increased physical connectivity between globules at higher ϕ_p or M_n could offset the field-induced reduction in total mesoglobule volume. This hypothesis is consistent with results at the highest polymer M_n (P314), where no change in hydrogel modulus with magnetization is observed at 7.5% P314 (Sec. SI.29). As this particular P314 polymer has a high dispersity (Đ= 3.03), a significant number of entanglements are present in solution at this concentration — further supporting that the impact of **B** fields is reduced as physical interactions in solution become dominant.

Other possible explanations for the observed **B** field-induced rheological behavior include a change in the inter-particle attractions or long-range repulsions between mesoglobules with magnetization. Minami et al. found that suspensions of PNIPAM microgel particles — which are structurally and rheologically similar to the suspensions of mesoglobules formed here (Ikeda et al. 2013; Pellet and Cloitre 2016; Scotti et al. 2020) — required the inter-particle charge repulsion to be suppressed for gelation to proceed (Minami et al. 2020). Thus if the **B** field promoted stronger inter-particle repulsions or weakened inter-globule attractions at higher temperatures, the resulting hydrogel modulus could be weakened. Based on Derjaguin, Landau, Verwey and Overbeek (DLVO) theory, the strength of the stabilizing repulsive interactions between PNIPAM mesoglobules depends upon the dielectric constant of the solvent. Pang and Deng (2008b) previously showed that **B** fields can increase the dielectric constant of water — potentially increasing the Debye screening length of PNIPAM mesoglobules and promoting stronger inter-particle repulsions. While possible, this explanation for **B**-induced hydrogel weakening is less plausible given that the initial rheological transition is nearly identical across field intensities for all examined polymer solutions — and changes in the inter-particle repulsions would likely alter this initial mesoglobule formation process and rheological transition (Neal et al. 2023b). Additionally, while weakened inter-globule attractions at higher temperatures would reduce G'_{max}, **B** fields have previously been shown to worsen solvent quality (Neal et al. 2023a; Vshivkov et al. 2017) — which should *increase*, not decrease, the strength of the inter-particle attractions at elevated temperatures. Thus the totality of the results herein — combined with evidence from prior work — suggest that magnetic fields weaken PNIPAM hydrogel formation by reducing the size and water content of magnetized mesoglobules.

Conclusion

The application of magnetic (**B**) fields during hydrogel formation in semi-dilute solutions (5–20% (w/w)) of thermoresponsive poly(N-isopropylacrylamide) (PNIPAM) weakens the resulting hydrogel strength in nearly all cases — except for in high molecular weight and dispersity PNIPAM (314 kDa, Đ~ 3.03). While **B** fields do not appear to significantly affect the initial steps of PNIPAM dehydration and aggregation as examined via oscillatory rheological temperature ramps, **B** fields hinder the formation of strong mesoglobule networks, resulting in much weaker hydrogels compared to those formed without **B** fields. Moreover, **B** fields can lower the maximum gelation temperature ($T_{G'_{max}}$) of 10% P59 considerably, up to 4.6 °C for field strengths of 0.6 T. This unusual magnetic field-induced hydrogel weakening strongly depends on magnetization time, with higher temperature ramp rates (shorter magnetization times) reducing the impact of the **B** field. While increasing temperature ramp rate appeared to reduce the magnetically induced weakening of 10% P59 hydrogels, pre-magnetization revealed that total time exposed to magnetic fields — rather than tempera-

ture ramp rate explicitly — is the most important parameter dictating the degree of hydrogel weakening.

The influence of **B** fields on PNIPAM gelation is also persistent across a range of polymer concentrations. Throughout the semi-dilute regime, **B** fields weaken the formation of mesoglobule networks and diminish the strength of physical hydrogels. Oscillatory amplitude sweeps reveal a two-step yielding mechanism characteristic of attractive-driven glasses (ADGs). These measurements confirm that the stresses corresponding to the breakage of both inter-mesoglobule linkages and caging restrictions decrease with field intensity. Further, the strain corresponding to the breakup of mesoglobule cages decreases with increasing field strength, suggesting a decrease in the length-scale of such restrictions. We propose that these changes in the hydrogel linear and nonlinear rheology are due to a field-induced reduction in the mesoglobule volume fraction. Specifically, based on the totality of the results and prior work, we propose that magnetic fields reduce both the PNIPAM mesoglobule size and water content — reducing both the hydrogel maximum modulus and temperature at which this maximum occurs. This study reveals that magnetic fields applied to diamagnetic polymer solutions have under-studied and profound impacts on macroscopic properties, unlocking new methods of directed assembly and polymer processing techniques.

Supplementary Information The online version contains supplementary material available at https://doi.org/10.1007/s00397-024-01454-y.

Acknowledgements The authors thank the Anton Paar VIP program for the rheometer and new tooling used in this work.

Author Contributions **Christopher A. P. Neal** and **Michelle A. Calabrese** wrote the manuscript. **Michelle A. Calabrese** supervised the research, and discussed data analysis and interpretation. **Christopher A. P. Neal** designed the experiments, and ran most turbidimetry, calorimetry and magnetorheology experiments. **Abhishek M. Shetty** assisted with development and procurement of the cone-and-plate geometry and discussed data analysis and interpretation. **Jason D. Linn** synthesized the PNIPAM polymer and discussed data analysis and interpretation. **Michelle C. Quan** and **Joseph D. Casas** ran supplementary turbidimetry and differential scanning calorimetry experiments.

Funding Research reported in this publication was primarily supported by the donors of ACS Petroleum Research Fund under Doctoral New Investigator Grant 65390-DNI7; M.A.C. served as Principal Investigator on ACS PRF# 65390-DNI7 that provided support for C.A.P.N and J.D.L. This research was also partially supported by the Office of the Vice President of Research, College of Science and Engineering, and the Department of Chemistry at the University of Minnesota. Research reported in this publication was supported by the Office of the Director, National Institutes of Health [Award Number S10OD011952]; the content is solely the responsibility of the authors and does not necessarily represent the official views of the National Institutes of Health. This work was supported partially by the Partnership for Research and Education in Materials (PREM) Program of the National Science Foundation under Award Number DMR-2122178, and through the University of Minnesota MRSEC under Award Number DMR-2011401 (J.D.C).

Data Availability All data generated or analyzed during this study are included in this published article and its supplementary information files. Datasets are also available from the corresponding author on reasonable request.

Declarations

Conflict of interest The authors declare no competing interests.

References

Ahuja A, Potanin A, Joshi YM (2020) Two step yielding in soft materials. Adv. Colloid Interfac. 282:102179. https://doi.org/10.1016/j.cis.2020.102179

Andrews R, Jacques D, Rao A, Rantell T, Derbyshire F, Chen Y, Haddon R (1999) Nanotube composite carbon fibers. Appl Phys Lett 75(9):1329–1331. https://doi.org/10.1063/1.124683

Aseyev V, Hietala S, Laukkanen A, Nuopponen M, Confortini O, Du Prez FE, Tenhu H (2005) Mesoglobules of thermoresponsive polymers in dilute aqueous solutions above the LCST. Polymer 46(18):7118–7131. https://doi.org/10.1016/j.polymer.2005.05.097

Asher SA, Holtz J, Liu L, Wu Z (1994) Self-Assembly Motif for Creating Submicron Periodic Materials Polymerized Crystalline Colloidal Arrays. J Am Chem Soc 116(11):4997–4998. https://doi.org/10.1021/ja00090a059

Smith AA, Maikawa CL, Hernandez HL, Appel EA (2021) Controlling properties of thermogels by tuning critical solution behaviour of ternary copolymers. Polym Chem 12(13):1918–1923. https://doi.org/10.1039/D0PY01696A

Bakherad M, Keivanloo A, Gholizadeh M, Doosti R, Javanmardi M (2017) Using magnetized water as a solvent for a green, catalyst-free, and efficient protocol for the synthesis of pyrano[2,3-c]pyrazoles and pyrano[4',3':5,6]pyrazolo [2,3-d]pyrimidines. Res Chem Intermed 43(2):1013–1029. https://doi.org/10.1007/s11164-016-2680-y

Balu C, Delsanti M, Guenoun P, Monti F, Cloitre M (2007) Colloidal Phase Separation of Concentrated PNIPAm Solutions. Langmuir 23(5):2404–2407. https://doi.org/10.1021/la0627821

Bischofberger I, Calzolari DCE, De Los Rios P, Jelezarov I, Trappe V (2014) Hydrophobic hydration of poly-N-isopropyl acrylamide: a matter of the mean energetic state of water. Sci Rep 4(1):4377. https://doi.org/10.1038/srep04377

Bischofberger I, Trappe V (2015) New aspects in the phase behaviour of poly-N-isopropyl acrylamide: systematic temperature dependent shrinking of PNiPAM assemblies well beyond the LCST. Sci Rep 5(1):15520. https://doi.org/10.1038/srep15520

Bohidar HB (2015) Concentration Regimes and Scaling. Fundamentals of Polymer Physics and Molecular Biophysics (pp. 150–168). Cambridge: Cambridge University Press

Bril M, Fredrich S, Kurniawan NA (2022) Stimuli-responsive materials: A smart way to study dynamic cell responses. Smart Mater. Med. 3:257–273. https://doi.org/10.1016/j.smaim.2022.01.010

Bulmus V, Ding Z, Long CJ, Stayton PS, Hoffman AS (2000) Site-Specific Polymer-Streptavidin Bioconjugate for pH-Controlled Binding and Triggered Release of Biotin. Bioconjugate Chem. 11(1):78–83. https://doi.org/10.1021/bc9901043

Buwalda SJ, Boere KWM, Dijkstra PJ, Feijen J, Vermonden T, Hennink WE (2014) Hydrogels in a historical perspective: From simple networks to smart materials. J Control Release 190:254–273. https://doi.org/10.1016/j.jconrel.2014.03.052

Cai R, Yang H, He J, Zhu W (2009) The effects of magnetic fields on water molecular hydrogen bonds. J Mol Struct 938(1):15–19. https://doi.org/10.1016/j.molstruc.2009.08.037

Cao Q, Rogers JA (2009) Ultrathin Films of Single-Walled Carbon Nanotubes for Electronics and Sensors: A Review of Fundamental and Applied Aspects. Adv Mater 21(1):29–53. https://doi.org/10.1002/adma.200801995

Chuang J, Grosberg AY, Tanaka T (2000) Topological repulsion between polymer globules. Chem Phys 112(14):6434–6442

Dai S, Ravi P, Tam KC (2008) pH-Responsive polymers: synthesis, properties and applications. Soft Matter 4(3):435–449. https://doi.org/10.1039/B714741D

de Gennes PG, Pincus PA (1970) Pair correlations in a ferromagnetic colloid. Z Phys B: Condens Matter 11(3):189–198. https://doi.org/10.1007/BF02422637

Esmaeilnezhad E, Choi HJ, Schaffie M, Gholizadeh M, Ranjbar M (2017) Characteristics and applications of magnetized water as a green technology. J. Cleaner Prod. 161:908–921. https://doi.org/10.1016/j.jclepro.2017.05.166

Filipcsei G, Csetneki I, Szilágyi A, Zrínyi M (2007) Magnetic Field-Responsive Smart Polymer Composites. Gong B, Sanford AR, Ferguson JS (Eds.), Oligomers - Polymer Composites - Molecular Imprinting (pp. 137–189). Berlin, Heidelberg: Springer

Forrest SR (2004) The path to ubiquitous and low-cost organic electronic appliances on plastic. Nature 428(6986):911–918. https://doi.org/10.1038/nature02498

Franco S, Buratti E, Nigro V, Zaccarelli E, Ruzicka B, Angelini R (2021) Glass and Jamming Rheology in Soft Particles Made of PNIPAM and Polyacrylic Acid. Int J Mol Sci 22(8):4032. https://doi.org/10.3390/ijms22084032

Garbern JC, Hoffman AS, Stayton PS (2010) Injectable pH- and Temperature-Responsive Poly(N-isopropylacrylamide-co-propylacrylic acid) Copolymers for Delivery of Angiogenic Growth Factors. Biomacromol 11(7):1833–1839. https://doi.org/10.1021/bm100318z

Ghorbani S, Ghorbani S, Tao Z, de Brito J, Tavakkolizadeh M (2019) Effect of magnetized water on foam stability and compressive strength of foam concrete. Constr Build Mater 197:280–290. https://doi.org/10.1016/j.conbuildmat.2018.11.160

Gopinadhan M, Majewski PW, Beach ES, Osuji CO (2012) Magnetic Field Alignment of a Diblock Copolymer Using a Supramolecular Route. ACS Macro Lett 1(1):184–189. https://doi.org/10.1021/mz2001059

Gorelov AV, Du Chesne A, Dawson KA (1997) Phase separation in dilute solutions of poly (N-isopropylacrylamide). Phys A 240(3):443–452. https://doi.org/10.1016/S0378-4371(97)00192-1

Granström M, Petritsch K, Arias AC, Lux A, Andersson MR, Friend RH (1998) Laminated fabrication of polymeric photovoltaic diodes. Nature 395(6699):257–260. https://doi.org/10.1038/26183

Halperin A, Kröger M, Winnik FM (2015) Poly(N-isopropylacrylamide) Phase Diagrams: Fifty Years of Research. Angew Chem Int Ed 54(51):15342–15367. https://doi.org/10.1002/anie.201506663

Hamley I, Castelletto V, Lu Z, Imrie C, Itoh T, Al-Hussein M (2004) Interplay between smectic ordering and microphase separation in a series of side-group liquid-crystal block copolymers. Macromol. 37(13):4798–4807. https://doi.org/10.1021/ma0498619

He L, Hu Y, Kim H, Ge J, Kwon S, Yin Y (2010) Magnetic Assembly of Nonmagnetic Particles into Photonic Crystal Structures. Nano Lett 10(11):4708–4714. https://doi.org/10.1021/nl103008v

Hoffman A, Stayton P, Bulmus V, Chen G, Chen J, Cheung C, Miyata T (2000) Really smart bioconjugates of smart polymers and receptor proteins. J Biomed Mater Res 52(4):577–586. https://doi.org/10.1002/1097-4636(20001215)52:4<577::AID-JBM1>3.0.CO;2-5

Holysz L, Szczes A, Chibowski E (2007) Effects of a static magnetic field on water and electrolyte solutions. J Colloid Interface Sci 316(2):996–1002. https://doi.org/10.1016/j.jcis.2007.08.026

Ikeda A, Berthier L, Sollich P (2013) Disentangling glass and jamming physics in the rheology of soft materials. Soft Matter 9(32):7669–7683. https://doi.org/10.1039/C3SM50503K

Jolly MR, Carlson JD, Muñoz BC (1996) A model of the behaviour of magnetorheological materials. Smart Mater Struct 5(5):607. https://doi.org/10.1088/0964-1726/5/5/009

Joshi RG, Tata BVR (2017) Sub-diffusive dynamics and two-step yielding in dense thermo-responsive microgel glasses. Colloid Polym Sci 295(9):1671–1683. https://doi.org/10.1007/s00396-017-4142-5

Kim D-H, Xiao J, Song J, Huang Y, Rogers JA (2010) Stretchable, Curvilinear Electronics Based on Inorganic Materials. Adv Mater 22(19):2108–2124. https://doi.org/10.1002/adma.200902927

Kimura T, Ago H, Tobita M, Ohshima S, Kyotani M, Yumura M (2002) Polymer composites of carbon nanotubes aligned by a magnetic field. Adv Mater 14(19):1380–1383. https://doi.org/10.1002/1521-4095(20021002)14:19<1380::AID-ADMA1380>3.0.CO;2-V

Kogure H, Nanami S, Masuda Y, Toyama Y, Kubota K (2005) Hydration and dehydration behavior of n-isopropylacrylamide gel particles. Colloid Polym Sci 283:1163–1171

Koumakis N, Petekidis G (2011) Two step yielding in attractive colloids: transition from gels to attractive glasses. Soft Matter 7(6):2456–2470. https://doi.org/10.1039/C0SM00957A

Krasovitski E, Cohen Y, Bianco-Peled H (2004) The effect of salts on the conformation and microstructure of poly (n-isopropylacrylamide)(pnipa) in aqueous solution. J. Polym. Sci. B Polym. Phys. 42(20):3713–3720

Kuijk A, van Blaaderen A, Imhof A (2011) Synthesis of Monodisperse, Rodlike Silica Colloids with Tunable Aspect Ratio. J Am Chem Soc 133(8):2346–2349. https://doi.org/10.1021/ja109524h

Kujawa P, Segui F, Shaban S, Diab C, Okada Y, Tanaka F, Winnik FM (2006) Impact of end-group association and main-chain hydration on the thermosensitive properties of hydrophobically modified telechelic poly (n-isopropylacrylamides) in water. Macromol. 39(1):341–348

Lang X, Patrick AD, Hammouda B, Hore MJA (2018) Chain terminal group leads to distinct thermoresponsive behaviors of linear PNIPAM and polymer analogs. Polym. 145:137–147. https://doi.org/10.1016/j.polymer.2018.04.068

Laurati M, Egelhaaf SU, Petekidis G (2011) Nonlinear rheology of colloidal gels with intermediate volume fraction. J Rheol 55(3):673–706. https://doi.org/10.1122/1.3571554

Lee H, Park TG (1998) Conjugation of Trypsin by Temperature-Sensitive Polymers Containing a Carbohydrate Moiety: Thermal Modulation of Enzyme Activity. Biotechnol Prog 14(3):508–516. https://doi.org/10.1021/bp9701224

Linn JD, Liberman L, Neal CAP, Calabrese MA (2022) Role of chain architecture in the solution phase assembly and thermoreversibility of aqueous PNIPAM/silyl methacrylate copolymers. Polym Chem 13(25):3840–3855. https://doi.org/10.1039/D2PY00254J

Liu J, Cao Y (2021) Experimental study on the surface tension of magnetized water. Int Commun Heat Mass Transfer 121:105091. https://doi.org/10.1016/j.icheatmasstransfer.2020.105091

Lu Y, Ye X, Li J, Li C, Liu S (2011) Kinetics of Laser-Heating-Induced Phase Transition of Poly(N-isopropylacrylamide) Chains in Dilute and Semidilute Solutions. J Phys Chem B 115(42):12001–12006. https://doi.org/10.1021/jp204853p

Maji S, Cesur B, Zhang Z, Geest BGD, Hoogenboom R (2016) Poly(N-isopropylacrylamide) coated gold nanoparticles as colourimetric temperature and salt sensors. Polym Chem 7(9):1705–1710. https://doi.org/10.1039/C5PY01959A

Mason TG, Weitz DA (1995) Linear Viscoelasticity of Colloidal Hard Sphere Suspensions near the Glass Transition. Phys Rev Lett 75(14):2770–2773. https://doi.org/10.1103/PhysRevLett.75.2770

Meier-Koll A, Pipich V, Busch P, Papadakis CM, Müller-Buschbaum P (2012) Phase separation in semidilute aqueous poly (n-isopropylacrylamide) solutions. Langmuir 28(23):8791–8798

Minami S, Yamamoto A, Oura S, Watanabe T, Suzuki D, Urayama K (2020) Criteria for colloidal gelation of thermo-sensitive poly(N-isopropylacrylamide) based microgels. J Colloid Interface Sci 568:165–175. https://doi.org/10.1016/j.jcis.2020.02.047

Neal CAP, Kresge GV, Quan MC, León V, Chibambo NO, Calabrese MA (2023) Effect of nanoparticle loading and magnetic field application on the thermodynamic, optical, and rheological behavior of thermoresponsive polymer solutions. J Vinyl Addit Technol 29(4):795–812. https://doi.org/10.1002/vnl.21968

Neal CAP, León V, Quan MC, Chibambo NO, Calabrese MA (2023) Tuning the thermodynamic, optical, and rheological properties of thermoresponsive polymer solutions via silica nanoparticle shape and concentration. J Colloid Interface Sci 629:878–895. https://doi.org/10.1016/j.jcis.2022.08.139

Niebuur B-J, Chiappisi L, Jung F, Zhang X, Schulte A, Papadakis CM (2019) Kinetics of Mesoglobule Formation and Growth in Aqueous Poly(N-isopropylacrylamide) Solutions: Pressure Jumps at Low and at High Pressure. Macromol. 52(17):6416–6427. https://doi.org/10.1021/acs.macromol.9b00937

Niebuur B-J, Lohstroh W, Appavou M-S, Schulte A, Papadakis CM (2019) Water dynamics in a concentrated poly (n-isopropylacrylamide) solution at variable pressure. Macromol. 52(5):1942–1954

Osuji C, Ferreira PJ, Mao G, Ober CK, Vander Sande JB, Thomas EL (2004) Alignment of Self-Assembled Hierarchical Microstructure in Liquid Crystalline Diblock Copolymers Using High Magnetic Fields. Macromol. 37(26):9903–9908. https://doi.org/10.1021/ma0483064

Osváth Z, Iván B (2017) The dependence of the cloud point, clearing point, and hysteresis of poly(n-isopropylacrylamide) on experimental conditions: The need for standardization of thermoresponsive transition determinations. Macromol Chem Phys 218(4):1600470. https://doi.org/10.1002/macp.201600470

Pan G, Kesavamoorthy R, Asher SA (1998) Nanosecond Switchable Polymerized Crystalline Colloidal Array Bragg Diffracting Materials. J Am Chem Soc 120(26):6525–6530. https://doi.org/10.1021/ja980481a

Pang X, Deng B (2008) Investigation of changes in properties of water under the action of a magnetic field. Sci China Ser G Phys Mech and Astro 51(11):1621–1632. https://doi.org/10.1007/s11433-008-0182-7

Pang XF (2006) The conductivity properties of protons in ice and mechanism of magnetization of liquid water. Eur Phys J B 49(1):5–23. https://doi.org/10.1140/epjb/e2006-00020-6

Pang X-F, Deng B (2008) The changes of macroscopic features and microscopic structures of water under influence of magnetic field. Phys B 403(19):3571–3577. https://doi.org/10.1016/j.physb.2008.05.032

Papadakis CM, Niebuur B-J, Schulte A (2024) Thermoresponsive Polymers under Pressure with a Focus on Poly(N-isopropylacrylamide) (PNIPAM). Langmuir 40(1):1–20. https://doi.org/10.1021/acs.langmuir.3c02398

Pellet C, Cloitre M (2016) The glass and jamming transitions of soft polyelectrolyte microgel suspensions. Soft Matter 12(16):3710–3720. https://doi.org/10.1039/C5SM03001C (Publisher: The Royal Society of Chemistry)

Peumans P, Forrest SR (2001) Very-high-efficiency double-heterostructure copper phthalocyanine/C60 photovoltaic cells. Appl Phys Lett 79(1):126–128. https://doi.org/10.1063/1.1384001

Peumans P, Uchida S, Forrest SR (2003) Efficient bulk heterojunction photovoltaic cells using small-molecular-weight organic thin films. Nature 425(6954):158–162. https://doi.org/10.1038/nature01949

Pham K, Egelhaaf S, Pusey P, Poon WC (2004) Glasses in hard spheres with short-range attraction. Phys Rev E 69(1):011503

Pham KN, Petekidis G, Vlassopoulos D, Egelhaaf SU, Poon WCK, Pusey PN (2008) Yielding behavior of repulsion- and attraction-dominated colloidal glasses. J Rheol 52(2):649–676. https://doi.org/10.1122/1.2838255

Philipp M, Kyriakos K, Silvi L, Lohstroh W, Petry W, Kruger JK, Muller-Buschbaum P (2014) From molecular dehydration to excess volumes of phase-separating pnipam solutions. J Phys Chem B 118(15):4253–4260

Pusey PN (2008) Colloidal glasses. J. Condens Matter Phys 20(49):494202. https://doi.org/10.1088/0953-8984/20/49/494202

Qiu X, Koga T, Tanaka F, Winnik FM (2013) New insights into the effects of molecular weight and end group on the temperature-induced phase transition of poly(N-isopropylacrylamide) in water. Sci China: Chem 56(1):56–64. https://doi.org/10.1007/s11426-012-4781-9

Ramon O, Kesselman E, Berkovici R, Cohen Y, Paz Y (2001) Attenuated total reflectance/fourier transform infrared studies on the phase-separation process of aqueous solutions of poly (n-isopropylacrylamide). J. Polym. Sci. B Polym. Phys. 39(14):1665–1677

Rogers SA, Erwin BM, Vlassopoulos D, Cloitre M (2011) A sequence of physical processes determined and quantified in LAOS: Application to a yield stress fluid. J Rheol 55(2):435–458. https://doi.org/10.1122/1.3544591

Ru G, Feng J (2011) Effects of end groups on phase transition and segmental mobility of poly(N-isopropylacrylamide) chains in D2O. J. Polym. Sci. B: Polym. Phys. 49(10):749–755. https://doi.org/10.1002/polb.22237

Saisavadas MV, Dhara S, Joshi RG, Tata BVR (2023) Large amplitude oscillatory shear studies on dense PNIPAM microgel colloidal glasses. Colloid Polym Sci 301(6):599–611. https://doi.org/10.1007/s00396-023-05096-z

Scotti A, Brugnoni M, Lopez CG, Bochenek S, Crassous JJ, Richtering W (2020) Flow properties reveal the particle-to-polymer transition of ultra-low crosslinked microgels. Soft Matter 16(3):668–678

Selim A-FH, El-Nady MF (2011) Physio-anatomical responses of drought stressed tomato plants to magnetic field. Acta Astronaut 69(7):387–396. https://doi.org/10.1016/j.actaastro.2011.05.025

Shah AA, Ganesan M, Jocz J, Solomon MJ (2014) Direct current electric field assembly of colloidal crystals displaying reversible structural color. ACS Nano 8(8):8095–8103. https://doi.org/10.1021/nn502107a

Shaheen SE, Brabec CJ, Sariciftci NS, Padinger F, Fromherz T, Hummelen JC (2001) 2.5% efficient organic plastic solar cells. Appl Phys Lett 78(6):841–843. https://doi.org/10.1063/1.1345834

Shangguan Y, Guo D, Feng H, Li Y, Gong X, Chen Q, Wu C (2014) Mapping phase diagrams of polymer solutions by a combination of microfluidic solution droplets and laser light-scattering detection. Macromol. 47(7):2496–2502. https://doi.org/10.1021/ma500056m

Shimizu T, Yamato M, Kikuchi A, Okano T (2001) Two-Dimensional Manipulation of Cardiac Myocyte Sheets Utilizing Temperature-Responsive Culture Dishes Augments the Pulsatile Amplitude. Tissue Eng 7(2):141–151. https://doi.org/10.1089/107632701300062732

Sronsri C, U-yen K, Sittipol W (2021) Analyses of vibrational spectroscopy, thermal property and salt solubility of magnetized water. J Mol Liq 323:114613. https://doi.org/10.1016/j.molliq.2020.114613

Takahashi T, Murayama T, Higuchi A, Awano H, Yonetake K (2006) Aligning vapor-grown carbon fibers in polydimethylsiloxane using dc electric or magnetic field. Carbon 44(7):1180–1188. https://doi.org/10.1016/j.carbon.2005.10.055

Tan Y, Xu K, Wang P, Li W, Sun S, Dong L (2010) High mechanical strength and rapid response rate of poly(N-isopropyl acrylamide) hydrogel crosslinked by starch-based nanospheres. Soft Matter 6(7):1467–1471. https://doi.org/10.1039/B916942C

Tanaka H (1992) Appearance of a moving droplet phase and unusual networklike or spongelike patterns in a phase-separating polymer solution with a double-well-shaped phase diagram. Macromol. 25(23):6377–6380. https://doi.org/10.1021/ma00049a042

Tanaka H (1993) Unusual phase separation in a polymer solution caused by asymmetric molecular dynamics. Phys Rev Lett 71(19):3158–3161. https://doi.org/10.1103/PhysRevLett.71.3158

Tavagnacco L, Zaccarelli E, Chiessi E (2018) On the molecular origin of the cooperative coil-to-globule transition of poly (n-isopropylacrylamide) in water. Phys Chem Chem Phys 20(15):9997–10010

Thévenot J, Oliveira H, Sandre O, Lecommandoux S (2013) Magnetic responsive polymer composite materials. Chem Soc Rev 42(17):7099–7116. https://doi.org/10.1039/C3CS60058K

Tokarev I, Minko S (2009) Multiresponsive, hierarchically structured membranes: new, challenging, biomimetic materials for biosensors, controlled release, biochemical gates, and nanoreactors. Adv Mater 21(2):241–247

Tong Z, Zeng F, Zheng X, Sato T (1999) Inverse Molecular Weight Dependence of Cloud Points for Aqueous Poly(N-isopropylacrylamide) Solutions. Macromol. 32(13):4488–4490. https://doi.org/10.1021/ma990062d

Uchida M, Sengoku T, Kaneko Y, Okumura D, Tanaka H, Ida S (2019) Evaluation of the effects of cross-linking and swelling on the mechanical behaviors of hydrogels using the digital image correlation method. Soft Matter 15(16):3389–3396. https://doi.org/10.1039/C9SM00049F

Van Durme K, Van Assche G, Van Mele B (2004) Kinetics of Demixing and Remixing in Poly(N-isopropylacrylamide)/Water Studied by Modulated Temperature DSC. Macromol. 37(25):9596–9605. https://doi.org/10.1021/ma048472b

Vshivkov SA, Rusinova EV, Klyuzhin ES, Kapitanov AA (2020) Effect of magnetic field on phase transitions and structure of polyelectrolyte solutions. Polym Sci Ser A Polym Phys 62(1):62–69. https://doi.org/10.1134/S0965545X19050183

Vshivkov SA, Zhernov IV, Nadol'skii AL, Mizyov AS (2017) Effect of magnetic field on phase transitions in solutions and melts of flexible polymers. Polym Sci Ser A Polym Phys 59(4):465–472. https://doi.org/10.1134/S0965545X17040149

Wang C, Hashimoto T, Chuang Y-C, Tanaka K, Chang Y-P, Yang T-W, Huang M-T (2022) Physical Gelation of Aqueous Solutions of Atactic Poly(N-isopropylacrylamide). Macromol. 55(20):9152–9167. https://doi.org/10.1021/acs.macromol.1c02476

Wang M, He L, Xu W, Wang X, Yin Y (2015) Magnetic assembly and field-tuning of ellipsoidal-nanoparticle-based colloidal photonic crystals. Angew Chem Int Ed 54(24):7077–7081. https://doi.org/10.1002/anie.201501782

Wang X, Qiu X, Wu C (1998) Comparison of the coil-to-globule and the globule-to-coil transitions of a single poly(n-isopropylacrylamide) homopolymer chain in water. Macromol. 31(9):2972–2976. https://doi.org/10.1021/ma971873p

Wang X, Wu C (1999) Light-scattering study of coil-to-globule transition of a poly(n-isopropylacrylamide) chain in deuterated water. Macromol. 32(13):4299–4301. https://doi.org/10.1021/ma9902450

Wang Y, Wei H, Li Z (2018) Effect of magnetic field on the physical properties of water. Results Phys. 8:262–267. https://doi.org/10.1016/j.rinp.2017.12.022

Wei M, Gao Y, Li X, Serpe JM (2017) Stimuli-responsive polymers and their applications. Polym Chem 8(1):127–143. https://doi.org/10.1039/C6PY01585A

Wu C, Li W, Zhu XX (2004) Viscoelastic Effect on the Formation of Mesoglobular Phase in Dilute Solutions. Macromol. 37(13):4989–4992. https://doi.org/10.1021/ma049556n

Wu C, Wang X (1998) Globule-to-coil transition of a single homopolymer chain in solution. Phys Rev Lett 80(18):4092–4094. https://doi.org/10.1103/PhysRevLett.80.4092

Wu C, Zhou S (1996) First observation of the molten globule state of a single homopolymer chain. Phys Rev Lett 77(14):3053–3055. https://doi.org/10.1103/PhysRevLett.77.3053

Xia L-W, Xie R, Ju X-J, Wang W, Chen Q, Chu L-Y (2013) Nano-structured smart hydrogels with rapid response and high elasticity. Nat Commun 4(1):2226. https://doi.org/10.1038/ncomms3226

Yanase K, Buchner R, Sato T (2020) Microscopic insights into the phase transition of poly(N-isopropylacrylamide) in aqueous media: Effects of molecular weight and polymer concentration. J Mol Liq 302:112025. https://doi.org/10.1016/j.molliq.2019.112025

Yushmanov PV, Furó I, Iliopoulos I (2006) Kinetics of Demixing and Remixing Transitions in Aqueous Solutions of Poly(N-isopropylacrylamide): A Temperature-Jump 1H NMR Study. Macromol Chem Phys 207(21):1972–1979. https://doi.org/10.1002/macp.200600394

Zaccarelli E, Poon WC (2009) Colloidal glasses and gels: The interplay of bonding and caging. Proc Natl Acad Sci USA 106(36):15203–15208

Zhao C, Yuan G, Han CC (2014) Bridging and caging in mixed suspensions of microsphere and adsorptive microgel. Soft Matter 10(44):8905–8912. https://doi.org/10.1039/C4SM01798F

Zhou Q, Qin B, Ma D, Jiang N (2017) Novel technology for synergetic dust suppression using surfactant-magnetized water in underground coal mines. Process Saf Environ Prot 109:631–638. https://doi.org/10.1016/j.psep.2017.05.013